JCB Journal of Cell Biology

ARTICLE

Maturation-driven transport and AP-1–dependent recycling of a secretory cargo in the Golgi

Jason C. Casler, Effrosyni Papanikou, Juan J. Barrero, and Benjamin S. Glick

Golgi cisternal maturation has been visualized by fluorescence imaging of individual cisternae in the yeast *Saccharomyces cerevisiae*, but those experiments did not track passage of a secretory cargo. The expectation is that a secretory cargo will be continuously present within maturing cisternae as resident Golgi proteins arrive and depart. We tested this idea using a regulatable fluorescent secretory cargo that forms ER-localized aggregates, which dissociate into tetramers upon addition of a ligand. The solubilized tetramers rapidly exit the ER and then transit through early and late Golgi compartments before being secreted. Early Golgi cisternae form near the ER and become loaded with the secretory cargo. As predicted, cisternae contain the secretory cargo throughout the maturation process. An unexpected finding is that a burst of intra-Golgi recycling delivers additional secretory cargo molecules to cisternae during the early-to-late Golgi transition. This recycling requires the AP-1 adaptor, suggesting that AP-1 can recycle secretory cargo proteins as well as resident Golgi proteins.

Introduction

Many features of the eukaryotic secretory pathway are well characterized. Soluble secretory cargo proteins are directed for translocation into the ER by an N-terminal signal sequence (Ng et al., 1996). After folding and assembly, newly synthesized secretory cargo proteins are packaged into COPII-coated vesicles at ER exit sites (ERES; Lord et al., 2013). Some secretory cargo proteins exit the ER by a nonselective bulk flow pathway, but many of them are concentrated in COPII vesicles with the aid of cargo receptors (Dancourt and Barlowe, 2010). After leaving the ER, secretory cargo proteins arrive in early (*cis*) cisternae of the Golgi apparatus, and then transit through the Golgi to late (*trans*) cisternae. In most cell types, the Golgi is organized as a stack of cisternae, and the secretory cargo proteins move in vectorial fashion across the stack (Dunphy and Rothman, 1985). Finally, secretory cargo proteins exit the Golgi in transport carriers for delivery to either the plasma membrane or the endosomal/lysosomal/vacuolar system (De Matteis and Luini, 2008).

The passage of secretory cargo proteins through the Golgi can be described by the cisternal maturation model (Glick and Nakano, 2009). According to this view, COPII vesicles fuse with one another to form early Golgi cisternae, which mature into late Golgi cisternae, which ultimately fragment into secretory vesicles and other types of transport carriers. During maturation of a cisterna, the secretory cargo proteins are continuously present but the population of resident Golgi proteins changes progressively. This change is thought to be driven by several mechanisms (Papanikou and Glick, 2014; Papanikou et al., 2015; Day et al., 2018). First, COPI-coated vesicles that bud from early cisternae transport resident Golgi proteins to other early cisternae or to the ER. Second, late Golgi proteins recycle to younger cisternae in clathrin-coated vesicles generated with the aid of the AP-1 adaptor. This AP-1–dependent recycling promotes the early-to-late Golgi transition. Third, peripheral membrane proteins dissociate from older cisternae and bind to younger cisternae. This model can explain how the Golgi transports diverse secretory cargoes, including large secretory cargoes that presumably must remain within the cisternae (Bonfanti et al., 1998).

Alternatively, other pathways have been postulated to operate in conjunction with or instead of cisternal maturation (Emr et al., 2009; Pfeffer, 2010; Glick and Luini, 2011). In mammalian cells, transient tubular connections between heterologous cisternae permit the rapid diffusion of some proteins across the Golgi stack (Beznoussenko et al., 2014). Additional suggested vehicles for the transport of secretory cargo proteins through the Golgi include anterograde COPI vesicles or large cisterna-derived membrane carriers (Orci et al., 2000; Pfeffer, 2010; Lavieu et al., 2013; Dunlop et al., 2017). Because of these different possibilities, further work is needed to characterize how cisternae mature, and to determine whether cisternal maturation can plausibly be considered the major pathway for transporting secretory cargo proteins through the Golgi.

Department of Molecular Genetics and Cell Biology, University of Chicago, Chicago, IL.

Correspondence to Benjamin S. Glick: bsglick@uchicago.edu.

The budding yeast *Saccharomyces cerevisiae* is a uniquely powerful model system for studying cisternal maturation. Unlike most other eukaryotes, *S. cerevisiae* has a nonstacked Golgi, meaning that individual Golgi cisternae are optically resolvable by fluorescence microscopy (Preuss et al., 1992; Wooding and Pelham, 1998; Beznoussenko et al., 2016). We and the Nakano group employed two-color 4D fluorescence microscopy to visualize cisternal maturation directly in living yeast cells (Losev et al., 2006; Matsuura-Tokita et al., 2006). For those experiments, resident Golgi proteins were fluorescently tagged, and individual cisternae were tracked over time to confirm that each cisterna exchanges early Golgi markers for late Golgi markers. Subsequent studies showed that normal Golgi maturation requires the actions of Rab GTPases and COPI, and that COPI and clathrin are recruited sequentially to maturing cisternae (Rivera-Molina and Novick, 2009; Daboussi et al., 2012; Papanikou et al., 2015; Ishii et al., 2016; Kim et al., 2016).

In contrast, for yeast secretory cargo proteins, tools for visualizing transport through the Golgi have been limited. Such tools have been used with mammalian cells to document that secretory cargo proteins arrive at the *cis* face of the Golgi and move through the stack to the *trans* face (Mironov et al., 2001; Trucco et al., 2004; Tie et al., 2016). The prediction is that in yeast, secretory cargo proteins should be continuously present within the Golgi cisternae as they mature. Such a phenomenon should be observable by three-color fluorescence microscopy in which an early Golgi marker, a late Golgi marker, and a secretory cargo are labeled in different colors. The secretory cargo should stay visible while the early Golgi marker departs and the late Golgi marker arrives (Fig. S1).

To test this fundamental prediction of the cisternal maturation model, we engineered a regulatable fluorescent secretory cargo that can be accumulated in the ER and then released for transport through the secretory pathway. The approach builds on a previously described technique in which a GFP-tagged monomeric secretory cargo was fused to four copies of a dimerizing mutant of the FK506-binding protein FKBP, leading to the formation of fluorescent aggregates in the ER lumen (Rivera et al., 2000). Those aggregates could be dissolved by addition of an FKBP ligand, thereby allowing the monomeric protein to exit the ER. In our version of this technique, an improved dimerizing mutant of FKBP is fused to a tetrameric red fluorescent protein, thereby generating fluorescent aggregates that can be dissolved to yield soluble tetramers (Barrero et al., 2016). By targeting such a construct to the ER lumen and appending an ER export signal (Nam et al., 2014), we generated a secretory cargo that can be induced to exit the ER rapidly and move through the Golgi. Three-color 4D microscopy confirmed that this secretory cargo remains continuously visible within maturing Golgi cisternae as predicted. Intriguingly, our data also indicate that the secretory cargo can recycle from older to younger cisternae during the early-to-late Golgi transition. The existence of such a recycling pathway could explain prior observations about the behavior of secretory cargo proteins in the Golgi.

Results

Designing a regulatable fluorescent secretory cargo for *S. cerevisiae*

The goal was to trap a fluorescent secretory cargo in the ER lumen and then release it for rapid transport through the secretory pathway. After exploring various approaches, including use of a thermosensitive COPII mutant to accumulate secretory cargo proteins in the ER (Castillon et al., 2009; Kurokawa et al., 2014), we chose to adapt a method that was previously developed for mammalian cells (Rivera et al., 2000). The highly soluble tetrameric red fluorescent protein DsRed-Express2 (Strack et al., 2008) was fused to a reversibly dimerizing variant of FKBP (Rollins et al., 2000; Barrero et al., 2016). An N-terminal signal sequence directs this fusion protein to the ER lumen, where it forms aggregates (Fig. 1 A). Addition of synthetic ligand of FKBP (SLF; Holt et al., 1993) disrupts FKBP dimerization and dissolves the aggregates, releasing soluble tetramers that can exit the ER (Fig. 1 A).

Although this approach is conceptually simple, implementation required careful engineering of the cargo and the yeast strain (Casler and Glick, 2018). A basic requirement was that the cargo aggregates must dissolve quickly and remain dissolved. We previously used rational mutagenesis to generate an improved reversibly dimerizing variant, here designated FKBPRD, which generates aggregates that dissolve within 1–2 min at low SLF concentrations (Barrero et al., 2016). FKBPRD has a cysteine at residue 22, prompting the concern that disulfide bonds could form in the ER lumen. Based on an alignment of FKBP homologues (Galat, 2008), we introduced a C22V mutation and confirmed that this mutation does not significantly alter the formation or dissolution of aggregates (Fig. S2 A). The resulting variant was designated FKBPRD(C22V). Another challenge was that yeast cells expel SLF by the action of pleiotropic drug transporters (Rogers et al., 2001). Removal of the transcription factors Pdr1 and Pdr3, which control the expression of many pleiotropic drug transporters (Schüller et al., 2007; Coorey et al., 2015), allows for sustained dissolution of aggregates in the presence of SLF (Barrero et al., 2016), so the strains used in this study contained the *pdr1Δ pdr3Δ* pair of gene deletions.

To ensure delivery of the DsRed-Express2-FKBPRD(C22V) construct to the ER lumen, we appended the Ost1 signal sequence, which efficiently directs cotranslational translocation (Willer et al., 2008; Fitzgerald and Glick, 2014; Barrero et al., 2018). The resulting construct was designated pOst1-DsRed-Express2-FKBPRD(C22V). After translocation, the Ost1 signal sequence should be removed by signal peptidase (Paetzel et al., 2002) to generate aggregation-prone DsRed-Express2-FKBPRD(C22V) tetramers in the ER lumen.

Expression of the pOst1-DsRed-Express2-FKBPRD(C22V) construct yielded red fluorescent aggregates, which were in the ER as judged by labeling the ER membrane with Erg11-GFP (Shakoury-Elizeh et al., 2010; Fig. 1 B). As a control, we examined pOst1-E2-Crimson-FKBP(C22V), which contained a far-red derivative of DsRed-Express2 (Strack et al., 2009b) fused to the monomeric FKBP(C22V) variant. No aggregates were seen with this construct. However, strong fluorescence was visible

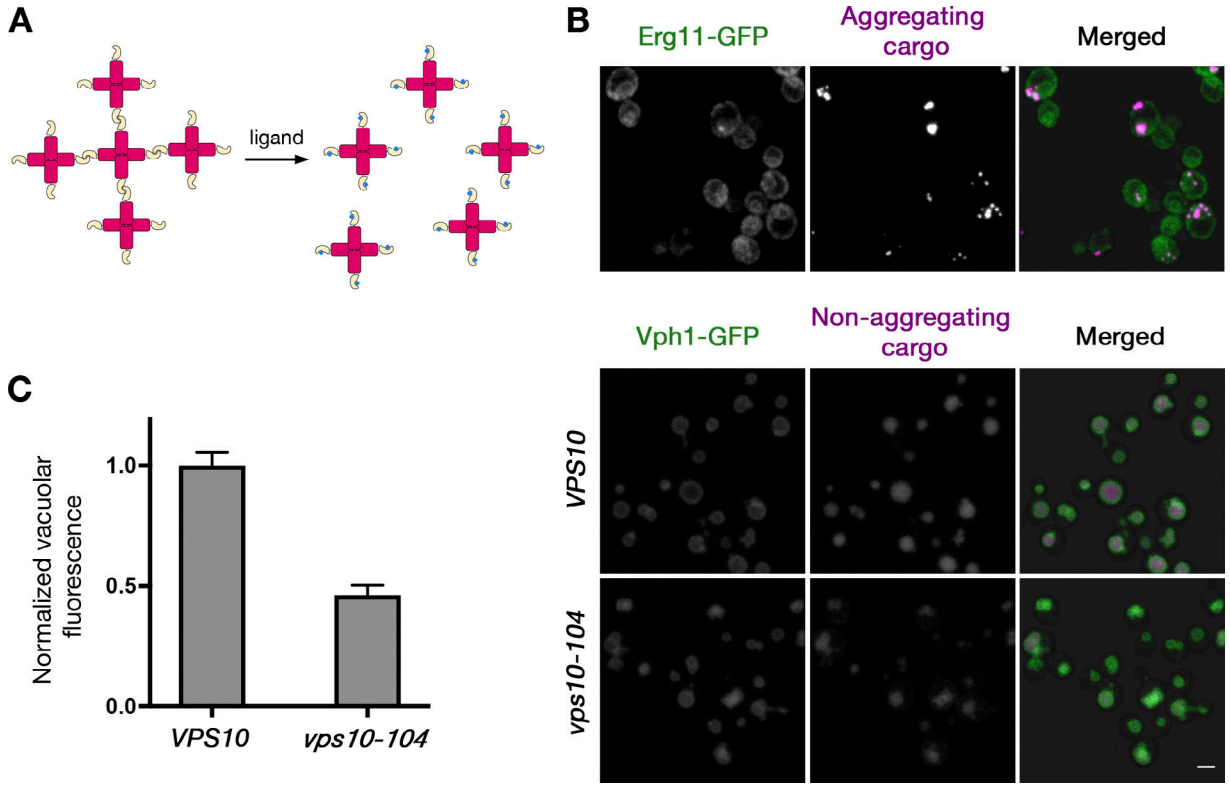

Figure 1. **A reversibly aggregating fluorescent secretory cargo. (A)** Strategy for generating and dissolving fluorescent aggregates. DsRed-Express2 tetramers (red) fused to a dimerizing variant of FKBP (gold) cross-link to form aggregates. Addition of the FKBP ligand SLF (blue) blocks dimerization, thereby dissolving the aggregates into soluble tetramers. **(B)** Dependence of aggregation on the dimerization of FKBP. A cargo construct containing the dimerizing FKBPRD(C22V) variant aggregated in the ER, which was marked by Erg11-GFP. By contrast, a cargo construct containing the monomeric FKBP(C22V) variant did not form ER aggregates, and the cargo was sorted to the vacuole, which was marked by Vph1-GFP. Introduction of the *vps10-104* mutation reduced the amount of the nonaggregating cargo in the vacuole. All images are projected confocal Z-stacks. Scale bar, 2 µm. **(C)** Quantification of the vacuolar fluorescence in B. For each cell, the green signal in the Vph1-GFP channel was used to create a mask for measuring the vacuolar fluorescence in the cargo channel. Data are average values from at least 110 cells for each strain. Error bars represent SEM.

in the vacuolar lumen as judged by labeling the vacuolar membrane with Vph1-GFP (Toshima et al., 2014; Fig. 1 B). We infer that after the E2-Crimson-FKBP(C22V) tetramers exited the ER, many of them were diverted to the vacuole. Sorting of fluorescent protein constructs to the *S. cerevisiae* vacuole can be inhibited by using the *vps10-104* allele (Jørgensen et al., 1999; Fitzgerald and Glick, 2014). Indeed, in a *vps10-104* strain, the vacuolar fluorescence seen with the pOst1-E2-Crimson-FKBP(C22V) construct was reduced (Fig. 1, B and C). The combined results suggested that expression of the pOst1-DsRed-Express2-FKBPRD(C22V) construct in a *pdr1Δ pdr3Δ vps10-104* strain would enable us to achieve regulated secretion of a fluorescent secretory cargo.

Accelerating secretion with an ER export signal

Addition of SLF was expected to dissolve the ER-localized DsRed-Express2-FKBPRD(C22V) aggregates, allowing soluble tetramers to diffuse throughout the ER. We added SLF using a custom flow chamber while performing 4D confocal imaging of the yeast cells (Barrero et al., 2016). The fluorescent DsRed-Express2-FKBPRD(C22V) aggregates dissolved within 1–2 min, yielding soluble red fluorescent molecules that filled the ER as judged by colabeling with Erg11-GFP (Video 1 and Fig. 2 A). No ER-localized aggregates reappeared in the presence of SLF, indicating that we had efficiently reversed the dimerization of FKBPRD(C22V).

Exit of the solubilized DsRed-Express2-FKBPRD(C22V) tetramers from the ER was slow, presumably because this secretory cargo lacks an ER export signal and therefore leaves the ER by bulk flow (Barlowe and Helenius, 2016). In attempts to accelerate ER export, we inserted different versions of the pro region of the yeast α-factor mating pheromone after the Ost1 signal sequence (Barrero et al., 2018) to provide a signal for binding to the ER export receptor Erv29 (Otte and Barlowe, 2004; Fitzgerald and Glick, 2014). Unfortunately, those constructs either aggregated irreversibly or failed to become trapped in the ER (data not shown). As a simpler alternative, we inserted only the first six residues of the α-factor pro region after the Ost1 signal sequence, thereby adding an N-terminal hexapeptide to each subunit of the DsRed-Express2-FKBPRD(C22V) tetramer. This hexapeptide has the sequence APVNTT. The NTT tripeptide is a signal for asparagine-linked glycosylation (Kornfeld and Kornfeld, 1985), which could potentially enhance ER export through interaction with lectin-like receptors in the ER (Sato and Nakano, 2002; Appenzeller-Herzog et al., 2005). Moreover, the N-terminal APV tripeptide is an evolutionarily conserved ER export signal (Nam et al., 2014; Yin et al., 2018).

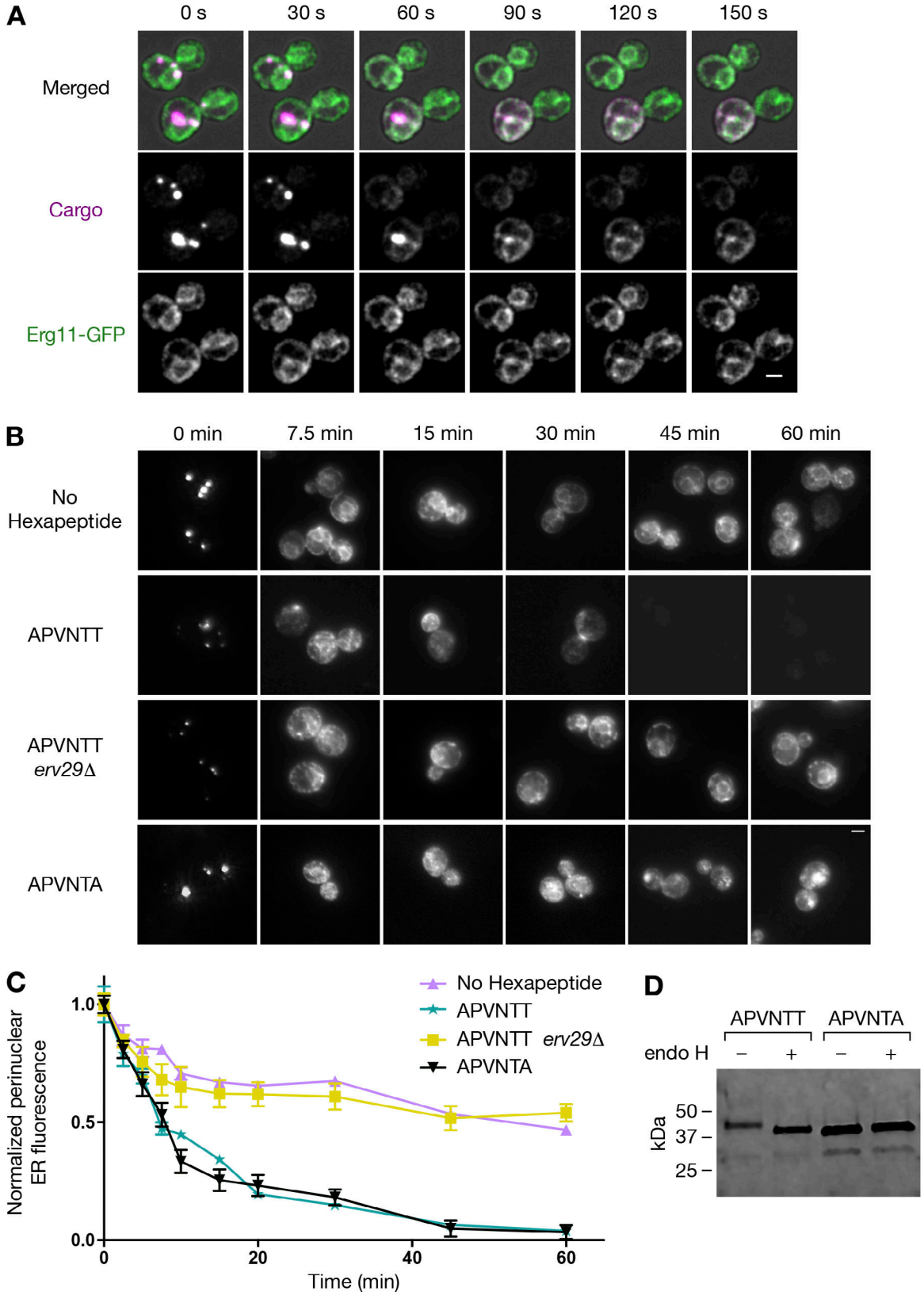

Figure 2. **Comparison of bulk flow-mediated versus signal-mediated ER export of fluorescent secretory cargo proteins. (A)** Projected Z-stacks from Video 1 showing the dissolution of cargo aggregates. Cells containing ER-localized aggregates of the DsRed-Express2-FKBPRD(C22V) cargo were mounted in a flow chamber and imaged while SLF-containing medium entered the chamber. The solubilized cargo colocalized with the ER marker Erg11-GFP. Scale bar, 2 µm. **(B)** Loss of ER-associated fluorescence for various cargo constructs after SLF addition. Strains expressed cargo variants with no export signal, the APVNTT hexapeptide, the APVNTA hexapeptide, or the APVNTT hexapeptide in an *erv29Δ* background. Growing cells were fixed at the indicated time points

after SLF addition, then imaged by wide-field fluorescence microscopy. Scale bar, 2 µm. **(C)** Quantification of the loss of ER-associated fluorescence in B. The perinuclear cargo signal was measured as described in Materials and methods. Plotted is the average fluorescence signal per unit area. Data were from 27–54 cells per time point, and error bars represent SEM. **(D)** Immunoblot to assess N-linked glycosylation of the cargo. Growing cells containing ER-localized aggregates of either the APVNTT-DsRed-Express2-FKBPRD(C22V) cargo or the APVNTA-DsRed-Express2-FKBPRD(C22V) cargo were lysed with glass beads and centrifuged, and the proteins released were precipitated. Resuspended samples were treated or mock treated with endo H, followed by SDS-PAGE and immunoblotting for FKBP. Numbers represent molecular weights of reference markers.

We therefore predicted that the APVNTT hexapeptide would accelerate ER export.

This prediction was tested by comparing the rates at which various solubilized tetramers exited the ER after SLF addition. The original pOst1-DsRed-Express2-FKBPRD(C22V) construct was compared with the pOst1-APVNTT-DsRed-Express2-FKBPRD(C22V) construct, which was presumably cleaved by signal peptidase to generate tetramers with the N-terminal hexapeptide. Two controls were also performed. First, the APVNTT sequence was changed to APVNTA to eliminate the signal for asparagine-linked glycosylation (Kornfeld and Kornfeld, 1985). Second, the pOst1-APVNTT-DsRed-Express2-FKBPRD(C22V) construct was expressed in an *erv29Δ* strain to prevent recognition of the ER export signal. The results are shown in Fig. 2 (B and C). In the absence of the hexapeptide, the DsRed-Express2-FKBPRD(C22V) tetramers exited the ER at the slow bulk flow rate, as indicated by a persistent fluorescence signal in the nuclear envelope portion of the ER. That persistent signal likely reflected a steady state in which slow ER exit was balanced by the accumulation of newly synthesized fluorescent molecules. In the presence of the hexapeptide, ER export was much faster, and the fluorescence signal in or near the nuclear envelope declined almost to zero with a half-time of ∼7.5 min. To confirm that the NTT signal resulted in asparagine-linked glycosylation, we showed that ER-localized molecules with the APVNTT hexapeptide had a slightly higher molecular weight than ER-localized molecules with the APVNTA hexapeptide, and that this difference was abolished by treatment with endoglycosidase H (endo H; Maley et al., 1989; Fig. 2 D). Nonglycosylated tetramers with the APVNTA hexapeptide exited the ER at the same rapid rate as glycosylated tetramers with the APVNTT hexapeptide, indicating that glycosylation was not primarily responsible for the accelerated ER export. By contrast, when the effect of the APV signal was eliminated by the *erv29Δ* mutation, ER export occurred at the slow bulk flow rate. Thus, the APVNTT hexapeptide allows for rapid Erv29-dependent ER export.

A potential drawback of our approach is that aggregated APVNTT-DsRed-Express2-FKBPRD(C22V) tetramers in the ER lumen could trigger the unfolded protein response (UPR), thereby perturbing the secretory pathway (Wu et al., 2014). To exclude this possibility, we examined *HAC1* mRNA, which is spliced upon activation of the UPR (Cox and Walter, 1996; Di Santo et al., 2016). As a control, DTT activated the UPR and generated a spliced form of *HAC1* mRNA (Fig. S2 B). Expression of the pOst1-APVNTT-DsRed-Express2-FKBPRD(C22V) construct did not trigger *HAC1* splicing (Fig. S2 B). This result indicates that the presence of aggregated APVNTT-DsRed-Express2-FKBPRD(C22V) tetramers is compatible with normal ER function.

After an APVNTT-DsRed-Express2-FKBPRD(C22V) tetramer assembles in the ER, there will be a kinetic race between aggregation and Erv29-dependent ER export. This interpretation is supported by Fig. S3. With the pOst1-APVNTT-DsRed-Express2-FKBPRD(C22V) construct, cells grown at 23°C or 30°C had abundant aggregates, but cells grown at 37°C had very few aggregates. If the APVNTT hexapeptide was absent, or if the strain carried an *erv29Δ* mutation, aggregates were seen even at 37°C (Fig. S3, A and B). The implication is that at 37°C, the relative kinetics of aggregation and Erv29-dependent ER export favored escape of APVNTT-containing tetramers from the ER. Even at 23°C or 30°C, many of the APVNTT-containing tetramers probably escaped the ER in an Erv29-dependent manner, because the total fluorescence from aggregates could be increased by removing the APVNTT hexapeptide or by deleting Erv29 (Fig. S3 C). Under the conditions of our experiments, which are performed at 23°C, there is evidently a balance such that aggregation of the APVNTT-DsRed-Express2-FKBPRD(C22V) tetramers is efficient enough to trap a fraction of the fluorescent secretory cargo molecules in the ER. Addition of SLF makes this population of molecules available for rapid ER export.

Compared with glycosylated tetramers with the APVNTT hexapeptide, nonglycosylated tetramers with the APVNTA hexapeptide yielded much stronger vacuolar labeling after prolonged incubation with SLF (Fig. 2 B). The strain carried the *vps10-104* mutation, so this effect of glycosylation involves a separate, unknown mechanism that may or may not be relevant for natural secretory cargo proteins. For our purposes, the empirical finding is that glycosylation helps to prevent the fluorescent secretory cargo from being diverted to the vacuole.

Tracking the fluorescent secretory cargo after ER export

At this point, we were ready to visualize the SLF-solubilized APVNTT-DsRed-Express2-FKBPRD(C22V) tetramers as they moved through the secretory pathway. The reference marker was the early Golgi protein GFP-Vrg4, the late Golgi protein Sec7-GFP, or the prevacuolar endosome (PVE) protein Vps8-GFP (Losev et al., 2006; Arlt et al., 2015; Day et al., 2018). This analysis was performed in strains that carried either the wild-type *VPS10* gene or the *vps10-104* allele. Cells were treated with SLF for 5 min, then fixed and imaged by two-color confocal microscopy. In the *VPS10* cells, the majority of the secretory cargo that was present in punctate structures colocalized with either the PVE marker or the early Golgi marker (Fig. 3, A and B). Only occasional colocalization was seen with the late Golgi marker. By contrast, in the *vps10-104* cells, colocalization with the PVE marker was minimal, and strong colocalization was seen with both the early and late Golgi markers (Fig. 3, A and B). These results support the view that the *vps10-104* mutation inhibits sorting of the secretory cargo to the PVE/vacuole system, thereby allowing the secretory cargo to traverse the entire Golgi for delivery to the cell surface.

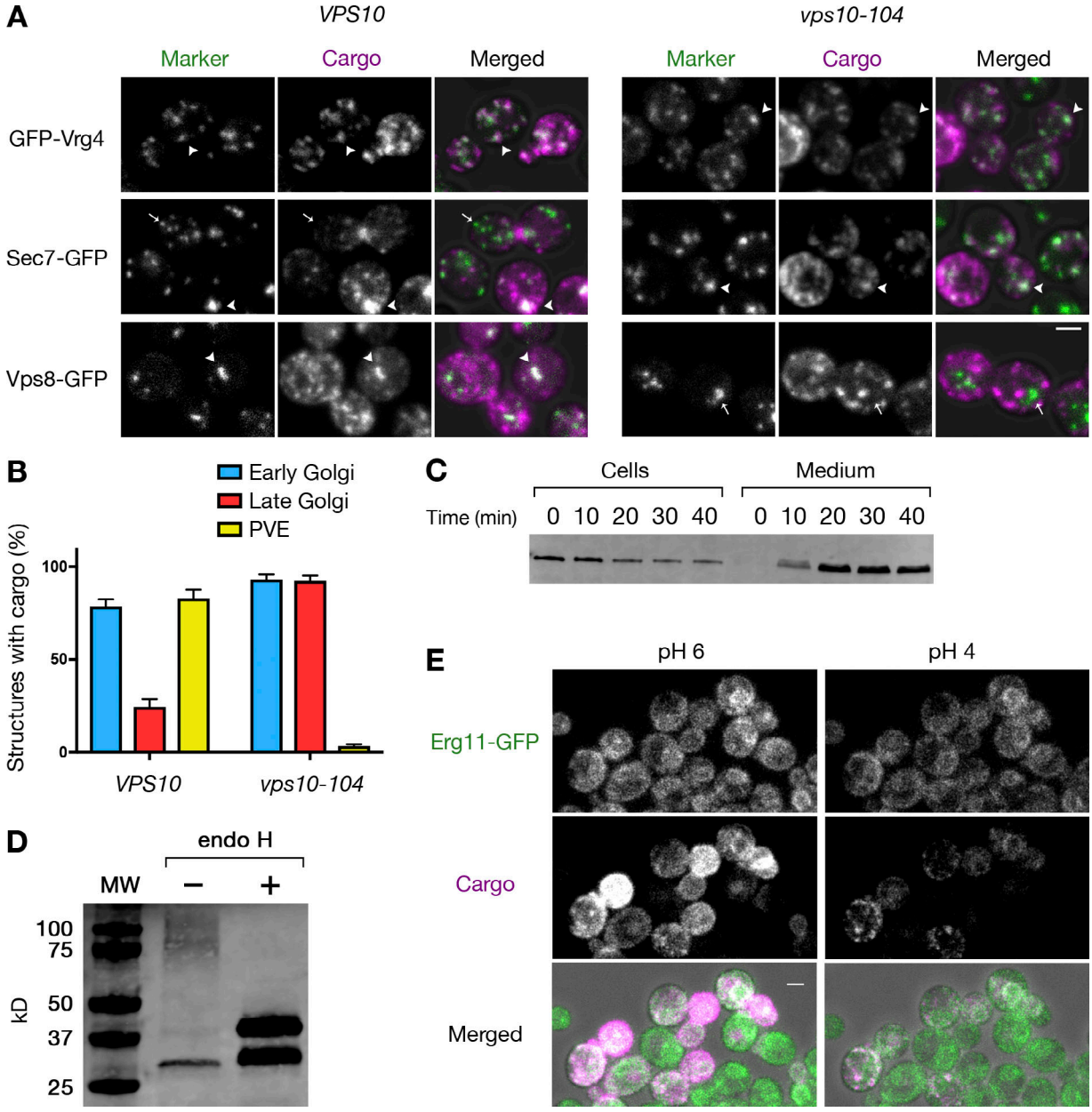

Figure 3. **Localization of the fluorescent secretory cargo after ER export. (A)** Colocalization of the cargo with Golgi and PVE markers soon after ER export. Cells expressing the APVNTT-DsRed-Express2-FKBPRD(C22V) cargo and either GFP-Vrg4 (early Golgi), Sec7-GFP (late Golgi), or Vps8-GFP (PVE) in a *pdr1Δ pdr3Δ* or *pdr1Δ pdr3Δ vps10-104* background were grown to mid-log phase, treated with SLF for 5 min, fixed, and imaged by confocal microscopy. Shown are representative projected Z-stacks. Arrowheads indicate examples of structures containing detectable cargo, and arrows indicate examples of structures lacking detectable cargo. Scale bar, 2 µm. **(B)** Quantification from A of the percentages of labeled structures containing detectable cargo. Data were obtained from at least 40 cells per condition. Error bars indicate SEM. **(C)** Immunoblot of cell-associated and secreted cargo after SLF addition in rich medium. Yeast were grown to mid-log phase in YPD, washed twice with fresh YPD, and treated with SLF. At the indicated time points, cell-associated and secreted fractions were separated by centrifugation, and then the sedimented cells were lysed and proteins from both fractions were precipitated. Samples were subjected to endo H treatment followed by SDS-PAGE and immunoblotting for FKBP. The visualized band corresponds to the upper band in the "+" lane of D. **(D)** Immunoblot demonstrating hyperglycosylation of the secreted cargo. Proteins were precipitated from rich medium 60 min after SLF addition. Samples were then treated or mock treated with endo H, followed by SDS-PAGE and immunoblotting for FKBP. A high-molecular-weight smear was seen only in the absence of endo H treatment. In the endo H–treated sample, the upper band is the full-length fusion protein, and the lower band is a minor species that was exaggerated by overloading the gel. The lower band might have been generated by Kex2 protease cleavage (Rockwell et al., 2002) of FKBP after the KR dipeptide at positions 17–18. MW, molecular weight marker, with the sizes of the reference proteins shown at the left. **(E)** Visualization of secreted cargo trapped in the periplasm in minimal medium. Cells expressing the aggregated cargo and the ER marker Erg11-GFP were grown to mid-log phase in NSD buffered at pH 6, then treated with SLF for 30 min and mounted in a flow chamber. Unbuffered NSD (pH ∼4) was flowed over the cells while imaging with a confocal microscope. Shown are projected Z-stacks from Video 2. Scale bar, 2 µm.

If the secretory cargo were being secreted as expected in a *vps10-104* strain, the cargo molecules should have appeared in either the periplasm or the medium or both, depending on how efficiently the cargo molecules escaped through the cell wall. In our previous work, an artificial yeast secretory cargo was more efficiently recovered from rich medium than from minimal medium (Fitzgerald and Glick, 2014), consistent with evidence that the *S. cerevisiae* cell wall is more permeable after growth in rich medium (De Nobel et al., 1990). The results described below support the same interpretation for the APVNTT-DsRed-Express2-FKBPRD(C22V) tetramers.

Secretion into the medium was measured by immunoblotting. When SLF was added to cells growing in minimal medium, no secretory cargo was detected in the medium by immunoblotting (data not shown). We therefore performed this experiment using rich medium. When SLF was added to cells growing in rich medium, the ER-localized aggregates dissolved, and the fluorescent secretory cargo appeared in the Golgi with kinetics similar to those observed in minimal medium (data not shown). The secretory cargo signal was visible in the rich medium by 10 min after SLF addition, and was more prominent by 20 min (Fig. 3 C). This time course was somewhat slower than expected, perhaps due to a delay in escape from the periplasm. The cargo molecules that remained in the cell pellet at later time points (Fig. 3 C) probably included tetramers that were trapped in the periplasm plus newly synthesized tetramers that were still in the secretory pathway. These results verify that the secretory cargo is indeed secreted, although quantitative analysis of the efficiency and kinetics of secretion would require removal of the cell wall (Gaynor and Emr, 1997).

The immunoblotting protocol used endo H treatment to eliminate smearing of the protein band due to variable glycosylation. When endo H treatment was omitted, the secreted cargo molecules were not seen as a tight band, but could be seen as a high-molecular-weight smear if the gel lane was overloaded (Fig. 3 D). The secretory cargo was evidently hyperglycosylated. Thus, the artificial secretory cargo behaves like glycoproteins that are naturally secreted by yeast cells (Trimble et al., 1983).

In minimal medium, most of the secreted cargo molecules presumably remained trapped in the periplasm. Because DsRed-Express2 fluorescence has a pK_a of ∼4.5 (Strack et al., 2009a), the signal can be quenched by acidification. When cells were grown in minimal medium buffered at pH 6, SLF addition resulted in the frequent appearance of red fluorescence around the rim of a bud or at the bud neck (Fig. 3 E). This signal was dramatically reduced by flowing in medium at pH 4.0 to quench DsRed-Express2 fluorescence (Video 2 and Fig. 3 E). We conclude that the fluorescent secretory cargo undergoes exocytosis at sites of polarized growth. Once again, this behavior is typical for secreted proteins in yeast (Field and Schekman, 1980; Finger and Novick, 1998).

The combined data indicate that APVNTT-DsRed-Express2-FKBPRD(C22V) acts as a regulatable secretory cargo in *vps10-104* cells. For the remainder of this study, the *vps10-104* allele was used, and the minimal medium was at pH 4.0 to suppress fluorescence from secreted cargo molecules in the periplasm.

Visualizing transport of the secretory cargo to the Golgi

According to the cisternal maturation model, Golgi cisternae are generated by the homotypic fusion of COPII vesicles that bud from ERES to carry secretory cargo proteins out of the ER (Glick and Nakano, 2009). This model makes two predictions that are pertinent for our analysis of *S. cerevisiae*. First, early Golgi cisternae should form near the ER. Second, the fluorescent secretory cargo should appear in newly formed early Golgi cisternae.

Do yeast Golgi cisternae form near the ER? Answering this question is tricky because chance alone gives a high probability that a cytoplasmic structure will be close to the nuclear envelope, the cortical ER, or the ER membranes that connect these two domains. To circumvent this problem, we added nocodazole for 2 h to generate cells that had large daughters lacking nuclei (Jacobs et al., 1988). The rationale was that the ER in those daughters was exclusively cortical, and the distance of a Golgi cisterna from the cortical ER was easy to measure. This approach was inspired by reports that nocodazole treatment does not perturb the yeast secretory pathway (Makarow, 1988; Vater et al., 1992). Indeed, our control experiments indicated that nocodazole had no effect on the average cisternal residence time of the early Golgi marker GFP-Vrg4 or the late Golgi marker Sec7-GFP (Fig. S4 A), the rate at which the fluorescent secretory cargo exited the ER (Fig. S4 B), or the appearance of the secretory cargo in rich medium after SLF addition (Fig. S4 C). We examined nucleus-free daughters in nocodazole-treated cells and measured the distance from the cortical ER during transitions in which Golgi cisternae acquired or lost either GFP-Vrg4 or Sec7-GFP. The results were striking (Fig. 4 C). Newly formed early Golgi cisternae acquired GFP-Vrg4 in close proximity to the cortical ER (average ER–Golgi distance of 0.21 µm, near the resolution limit of our imaging system). By contrast, older Golgi cisternae lost GFP-Vrg4, and acquired and lost Sec7-GFP, throughout the daughter (average ER–Golgi distance of 0.44–0.61 µm). When early Golgi cisternae were tracked during the period in which they contained GFP-Vrg4, many of them could be seen to move away from the cortical ER (Video 3 and Fig. 4, A and B). We conclude that early Golgi cisternae form near the ER and then dissociate from sites of cisternal assembly.

The next step was to visualize the early trafficking of the fluorescent secretory cargo. Addition of SLF quickly dissolved the aggregates, but unlike the DsRed-Express2-FKBPRD(C22V) cargo visualized in Fig. 2 A, the APVNTT-DsRed-Express2-FKBPRD(C22V) cargo immediately began to concentrate in punctate structures. To characterize those structures, we labeled the early Golgi with GFP-Vrg4 and simultaneously labeled ERES by tagging the COPII coat protein Sec31 with HaloTag conjugated to the far-red dye JF_{646} (Rossanese et al., 1999; Grimm et al., 2015; Day et al., 2018). The cargo-containing punctate structures were consistently next to ERES but were less numerous than ERES (Fig. S5). A cargo-containing punctate structure was associated in some cases with a single ERES and in other cases with multiple ERES. This observation might mean that several ERES could export cargo to the same punctate structure, although due to the large number of ERES in *S. cerevisiae* cells (Rossanese et al., 1999), some of the associations were probably coincidental.

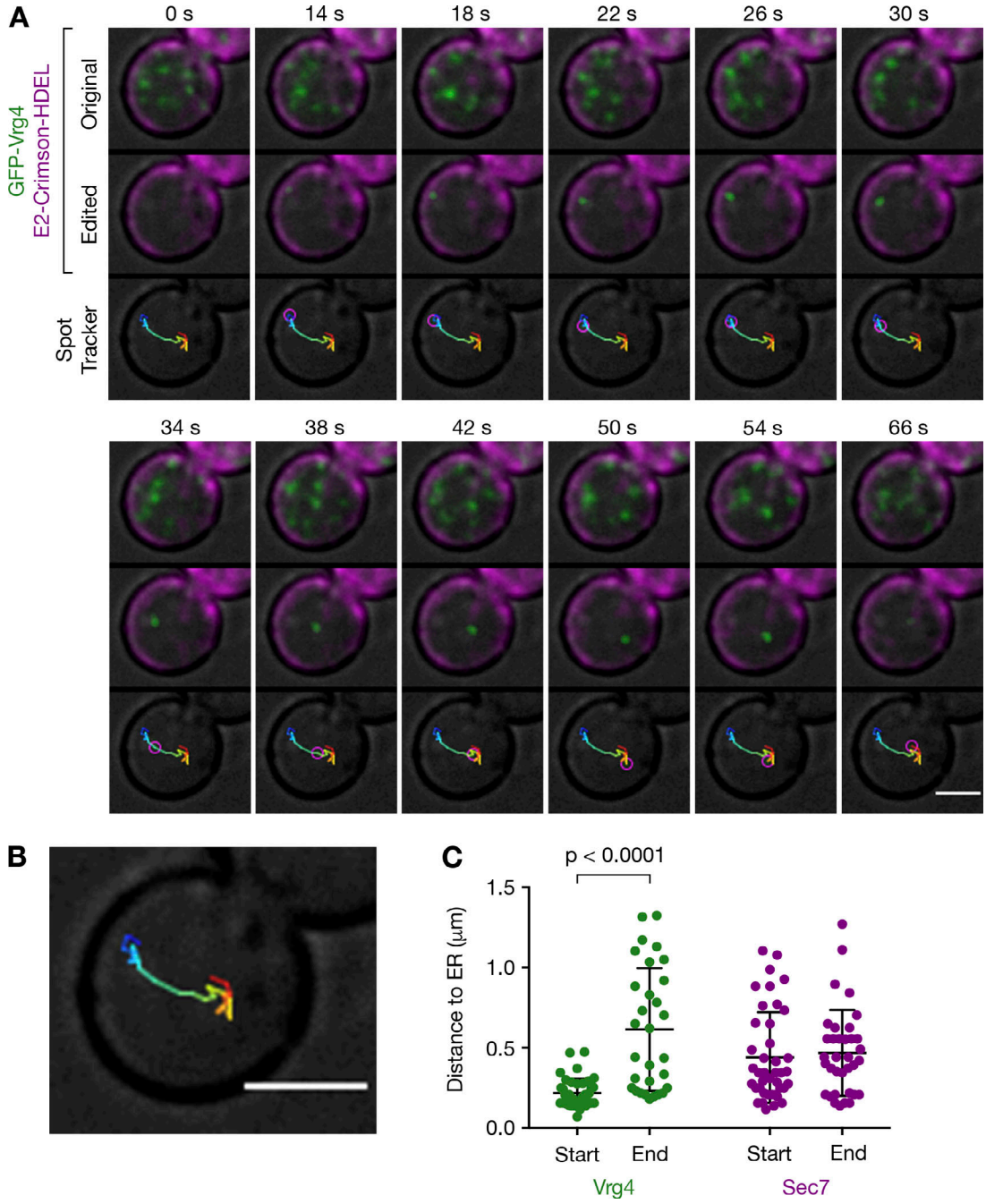

Figure 4. **Formation of new Golgi cisternae near the ER in nocodazole-treated cells. (A)** Tracking of a representative early Golgi cisterna. The early Golgi was labeled with GFP-Vrg4, and the ER lumen was labeled with E2-Crimson-HDEL (Strack et al., 2009b). From Video 3, the top row is a projection of optical sections from the center of the cell, the middle row is the same projection after editing to highlight the tracked cisterna, and the bottom row illustrates the path followed by the tracked cisterna. Scale bar, 2 µm. **(B)** Enlargement of the track from part A. Time is indicated by a gradient from blue to red. Scale bar, 2 µm. **(C)** Quantification of the distances between cisternae and the ER during the arrival (Start) and departure (End) of early and late Golgi markers. Strains contained E2-Crimson-HDEL, together with either GFP-Vrg4 (early Golgi) or Sec7-GFP (late Golgi). Cells were grown to mid-log phase, treated with nocodazole for 2 h, and imaged by 4D confocal microscopy. Measurements were derived from the daughters, which lacked perinuclear ER fluorescence. Each of the chosen cisternae experienced a transition in GFP-Vrg4 or Sec7-GFP labeling while near the center of the cell along the vertical axis. At the time of a transition, 8–12 optical sections from the center of the cell were projected, and the distance to the cortical ER was measured using the Line tool in ImageJ. The scatter plot for a transition shows the mean distance from the ER and the standard deviation. For each condition, data were taken from events in at least 30 different cells visualized in seven or more videos. To determine statistical significance, the Vrg4 datasets were compared using the Mann–Whitney *U* test.

Many ERES were distant from the cargo-containing punctate structures (Fig. S5), implying that only a subset of the ERES were active at a given time, or that different ERES were exporting distinct classes of proteins (Castillon et al., 2009). Each cargo-containing punctate structure either labeled with GFP-Vrg4 or soon acquired GFP-Vrg4 (Video 4 and Fig. 5 A). Taken together,

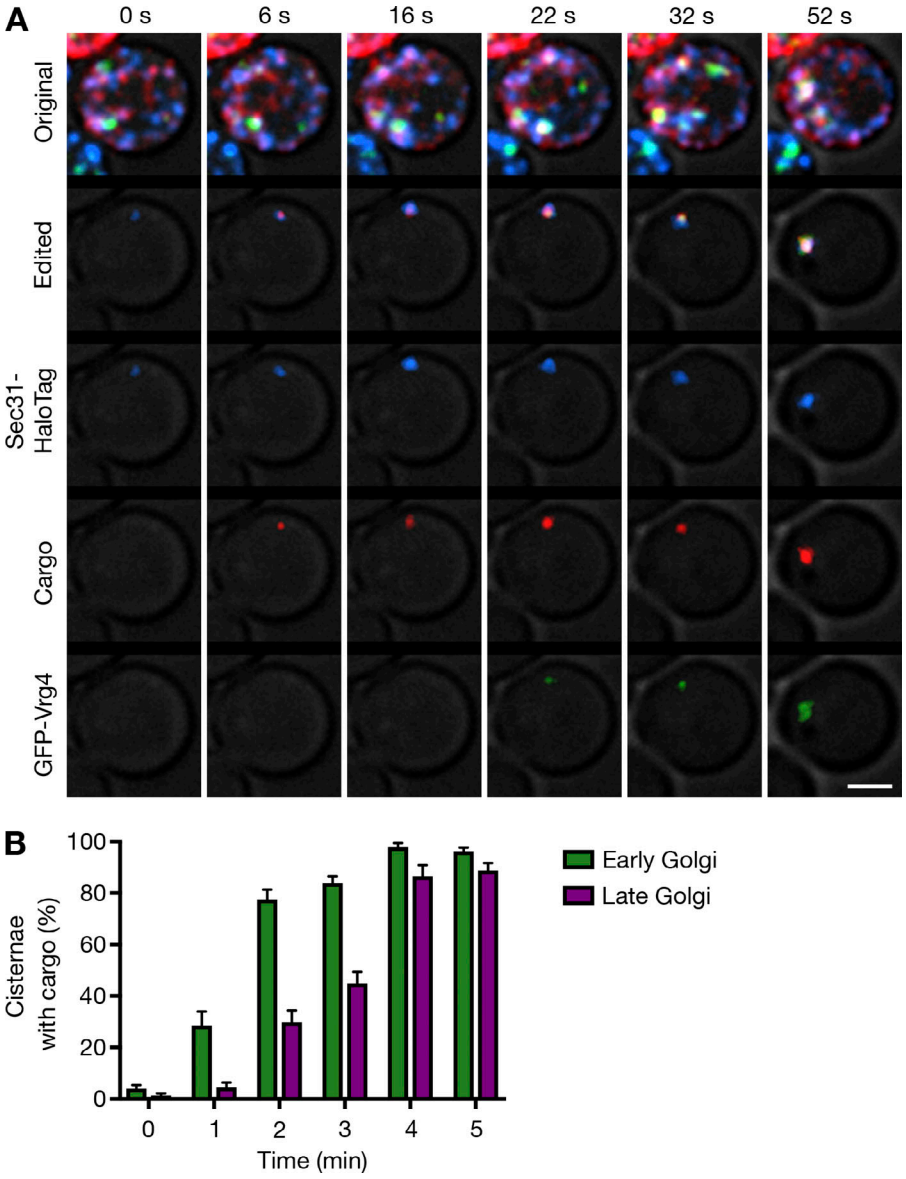

Figure 5. **Traffic of the fluorescent secretory cargo to Golgi compartments. (A)** Concentration of the cargo in a nascent Golgi cisterna that formed near an ERES. A strain expressing the APVNTT-DsRed-Express2-FKBPRD(C22V) cargo together with Sec31-HaloTag (ERES) and GFP-Vrg4 (early Golgi) was imaged by 4D microscopy during and after addition of SLF in a flow chamber. Depicted here is a representative example of the results, in frames from Video 4. The top row is the complete projection, the second row is the same projection after editing to highlight the tracked compartments, and the remaining three rows are the individual channels for the edited projection. Time zero represents ∼45 s after the cells were exposed to SLF. The solubilized cargo became concentrated in a structure that was near an ERES, and then GFP-Vrg4 arrived at the same structure. Scale bar, 2 µm. **(B)** Sequential appearance of the cargo in early and then late Golgi cisternae. Cells expressing the aggregated cargo together with GFP-Vrg4 (early Golgi) and Sec7-HaloTag (late Golgi) were grown to mid-log phase, labeled with JF_{646}, and imaged by 4D confocal microscopy while flowing in medium containing SLF. Movies were analyzed by quantifying the percentages of the early and late Golgi cisternae that contained detectable cargo at the indicated time points. Data were taken from 27 cells in seven videos. Error bars represent SEM.

these results indicate that after SLF addition, the fluorescent secretory appeared in early Golgi cisternae that had formed next to ERES.

Visualizing the behavior of the secretory cargo during Golgi maturation

An obvious prediction was that during the wave of fluorescent secretory cargo transport, the cargo should be visible first in the early Golgi and then in the late Golgi. To test this idea, we analyzed cells at various times after SLF addition and counted the percentages of early and late Golgi cisternae that contained detectable amounts of fluorescent secretory cargo. Labeling of the early Golgi cisternae was nearly maximal after 2 min, whereas labeling of the late Golgi cisternae was maximal after 4 min (Fig. 5 B). Thus, the secretory cargo moved progressively through the Golgi.

We were now prepared to carry out the key experiment of visualizing the fluorescent secretory cargo in maturing Golgi cisternae. For this purpose, the secretory cargo was expressed in a strain that contained GFP-Vrg4 together with Sec7-HaloTag conjugated to JF_{646}. Consistent with our earlier findings (Losev et al., 2006; Papanikou et al., 2015), individual cisternae acquired GFP-Vrg4, then lost GFP-Vrg4 as they acquired Sec7-HaloTag, and then lost Sec7-HaloTag, all over a time course of ∼3 min. The presence of the fluorescent secretory cargo did not detectably alter Golgi morphology or maturation dynamics. Secretory cargo fluorescence was reproducibly visible throughout the period in which a cisterna contained early and late Golgi markers (Video 5 and Fig. 6 A). These data are quantified in Fig. 6 B for the two cisternae analyzed in Video 5. Our results verify the basic prediction that a secretory cargo should be present within maturing cisternae as the resident Golgi proteins come and go.

Interestingly, we often saw that the amount of fluorescent secretory cargo in a cisterna increased around the time of the early-to-late transition, and then decreased during the late stage

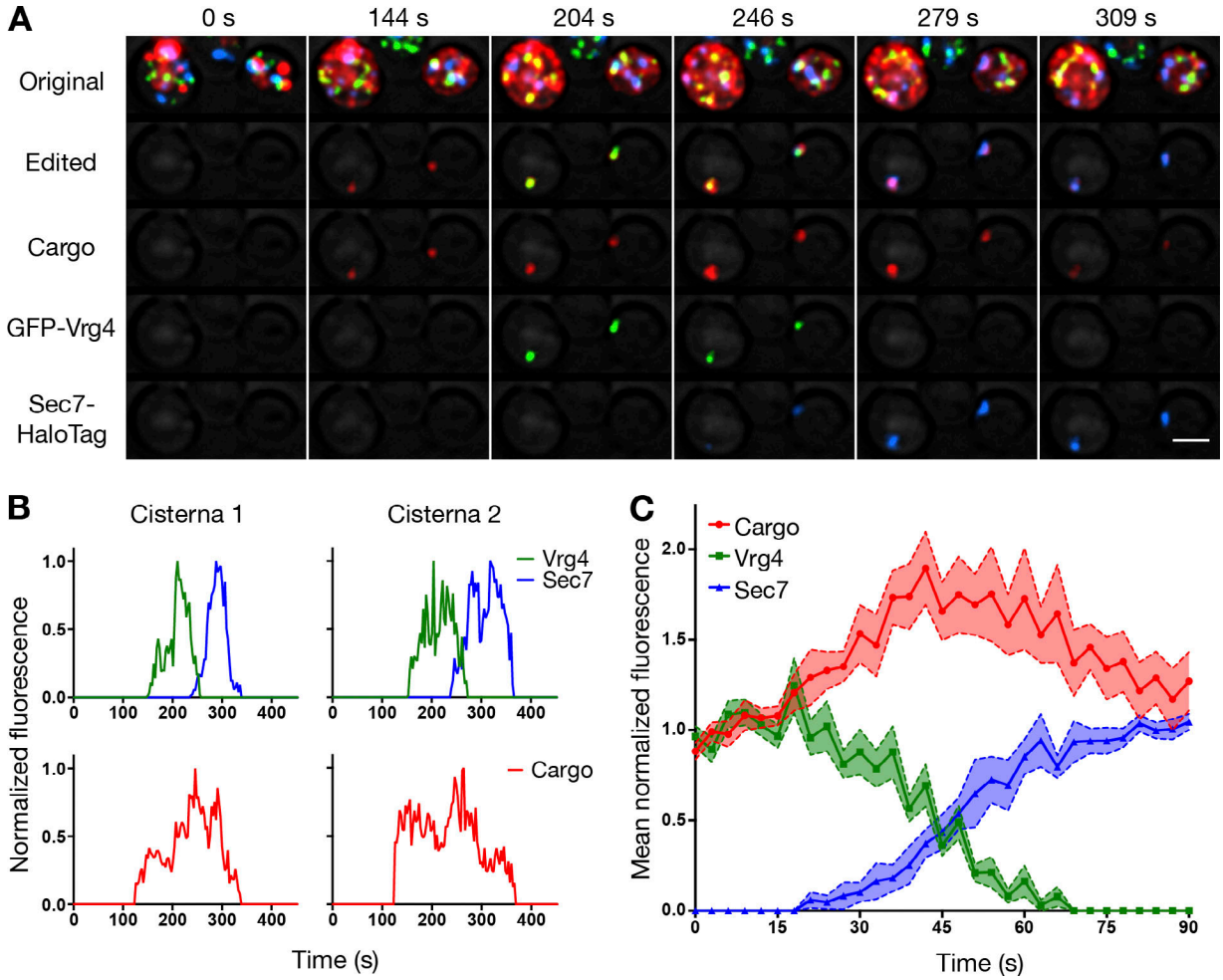

Figure 6. **Persistence of the fluorescent secretory cargo in maturing Golgi cisternae. (A)** Visualization of the cargo in maturing Golgi cisternae. Cells expressing the APVNTT-DsRed-Express2-FKBPRD(C22V) cargo together with GFP-Vrg4 (early Golgi) and Sec7-HaloTag (late Golgi) were grown to mid-log phase, labeled with JF_{646}, and imaged by 4D confocal microscopy while flowing in medium containing SLF. Shown are projected Z-stacks from the representative data in Video 5. The top row is the complete projection, the second row is the same projection after editing to highlight the two cisternae that were tracked, and the remaining three rows are the individual channels for the edited projection. Scale bar, 2 µm. **(B)** Quantification of the fluorescence intensities of Golgi markers and cargo during typical maturation events. The graphs represent the cisternae tracked in A, with the signals normalized to a maximum value of 1.0. **(C)** Average cargo signal change during the early-to-late Golgi transition. For each of 19 separate maturation events, fluorescence was quantified over a period of 90 s with Z-stacks collected every 3 s. Normalization of a trace was performed by defining 1.0 as the average of the first six fluorescence values for Vrg4 or the cargo, or as the average of the last six fluorescence values for Sec7. Traces were aligned at the midpoints of the Vrg4-to-Sec7 transitions, and the normalized fluorescence signals were averaged. The shaded borders indicate SEM.

of maturation (Fig. 6 B). The transient increase raised the signal by an average of ∼70% (Fig. 6 C). This phenomenon could reflect vesicular transport of secretory cargo molecules between cisternae. To test this possibility, we used FRAP to bleach the secretory cargo molecules in early Golgi cisternae while leaving the resident Golgi markers unaffected, and then tracked the cisternae as they matured to detect any recovery of the secretory cargo signal. For convenience, this experiment was performed with nocodazole-treated cells, and all of the cargo fluorescence in a large daughter was bleached simultaneously. Identification of the daughter was unambiguous because the mother had brighter cargo fluorescence due to the presence of nuclear ER. Intense laser illumination of the daughter began 3 min after SLF addition and persisted for 40 s to ensure complete bleaching. The mother and daughter cytoplasms were interconnected, so vesicles carrying fluorescent secretory cargo molecules from the mother could potentially replenish the bleached cisternae in the daughter. For each early Golgi cisterna that we could track, there was an initial period during which cargo fluorescence showed no recovery, followed by a sudden return of cargo fluorescence around the time of the early-to-late transition (Video 6 and Fig. 7). We calculated the predicted level of fluorescence recovery as follows. In unbleached cells, cargo fluorescence increased by ∼70% during the early-to-late transition, suggesting that ∼70 of 170 or 40% of the secretory cargo molecules in late Golgi cisternae originated from other cisternae. In a FRAP experiment, approximately half of the secretory cargo molecules that arrive from other cisternae will have been rendered nonfluorescent by bleaching the daughter, so the recovered cargo fluorescence in the bleached cisternae should be on the order of 20% of the

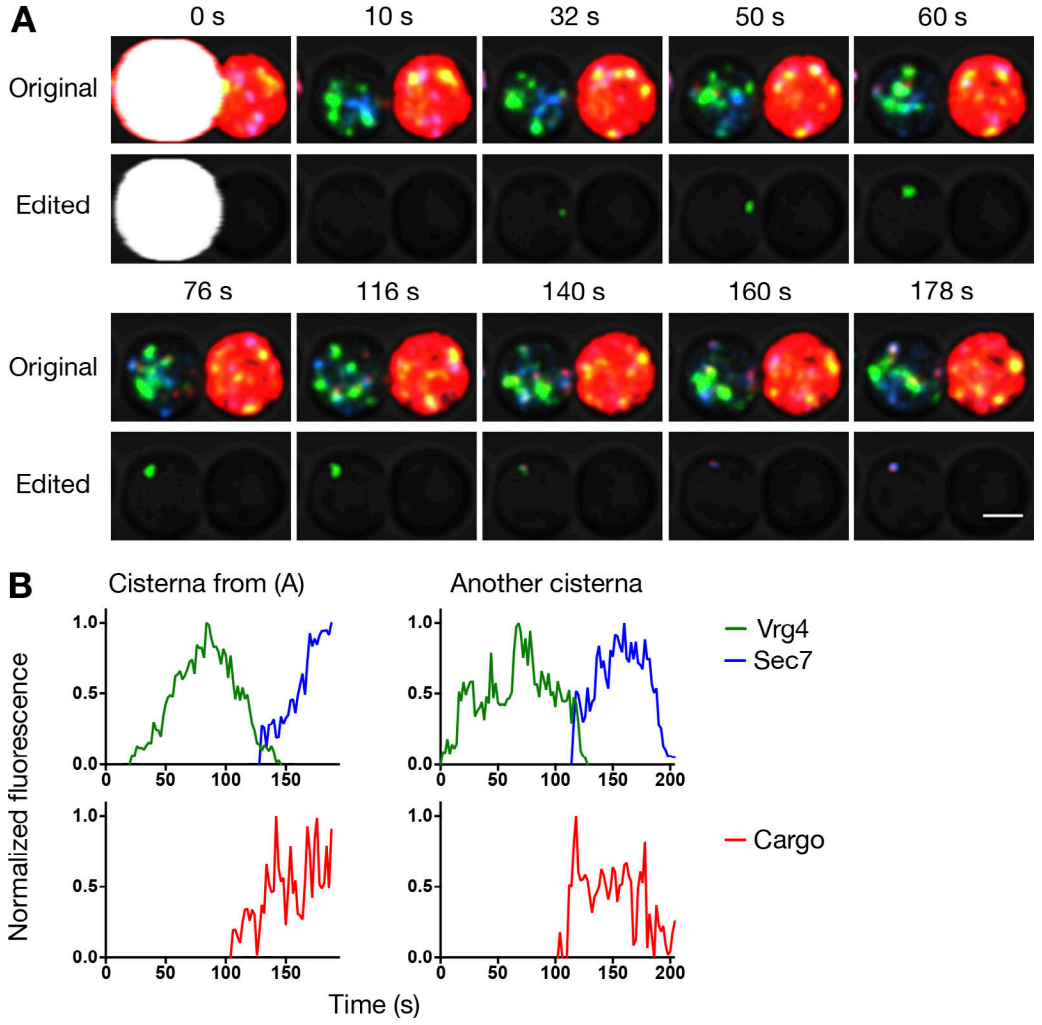

Figure 7. **Arrival of fluorescent secretory cargo molecules during the early-to-late Golgi transition. (A)** Visualizing traffic of the cargo to maturing cisternae. Cells expressing the APVNTT-DsRed-Express2-FKBPRD(C22V) cargo together with GFP-Vrg4 (early Golgi) and Sec7-HaloTag (late Golgi) were grown to mid-log phase, treated with nocodazole for 2 h, labeled with JF_{646}, and imaged by 4D confocal microscopy. SLF was added for 3 min to enable early Golgi cisternae to become loaded with cargo. At that point, the cargo fluorescence in an entire daughter was bleached by illuminating with the laser at maximum intensity for ∼40 s. Then individual cisternae in the daughter were tracked as in Fig. 6 A by following the Golgi markers, which were not affected by the bleaching. Shown are projected Z-stacks from the representative data in Video 6. The top row is the complete projection, and the bottom row is the same projection after editing to highlight the cisterna that was tracked. Scale bar, 2 µm. **(B)** Quantification of the Golgi markers and the fluorescence recovery of the cargo during typical maturation events in a daughter after cargo bleaching. The first graph represents the cisterna tracked in A, and the second graph represents another typical cisterna tracked in a similar video. These data from two videos are representative of four total videos analyzed. As a control, when both the mother and daughter were bleached, no fluorescence recovery of the cargo was seen (not depicted).

normal cargo fluorescence in unbleached cisternae. Indeed, by the time a cisterna showed maximal labeling with Sec7-HaloTag, the cargo fluorescence in the cisternae that had been bleached averaged ∼25% of the level seen for cisternae in unbleached nocodazole-treated daughters (Fig. 8 B). These results are evidence for a burst of incoming secretory cargo traffic as an early cisterna matures into a late cisterna.

Probing the mechanism of secretory cargo transport between cisternae

For two reasons, we suspected that the carriers responsible for transporting the fluorescent secretory cargo between cisternae might be vesicles generated with the aid of the heterotetrameric AP-1 clathrin adaptor (Myers and Payne, 2013). First, arrival of secretory cargo molecules occurred during the early-to-late transition, and AP-1 apparently mediates intra-Golgi recycling from late to transitioning cisternae (Papanikou et al., 2015; Day et al., 2018). Second, the secretory cargo signal in a cisterna typically declined after the early-to-late transition, consistent with the idea that late Golgi cisternae were exporting fluorescent secretory cargo molecules to younger cisternae. To test this hypothesis, we deleted the Apl4 subunit of the AP-1 adaptor. Remarkably, in an *apl4Δ* strain, there was no increase in the amount of fluorescent secretory cargo during the early-to-late transition (Fig. 8 A) and no recovery of cargo fluorescence in bleached cisternae (Fig. 8 B). Our results are consistent with a role for AP-1 in recycling the fluorescent secretory cargo between cisternae.

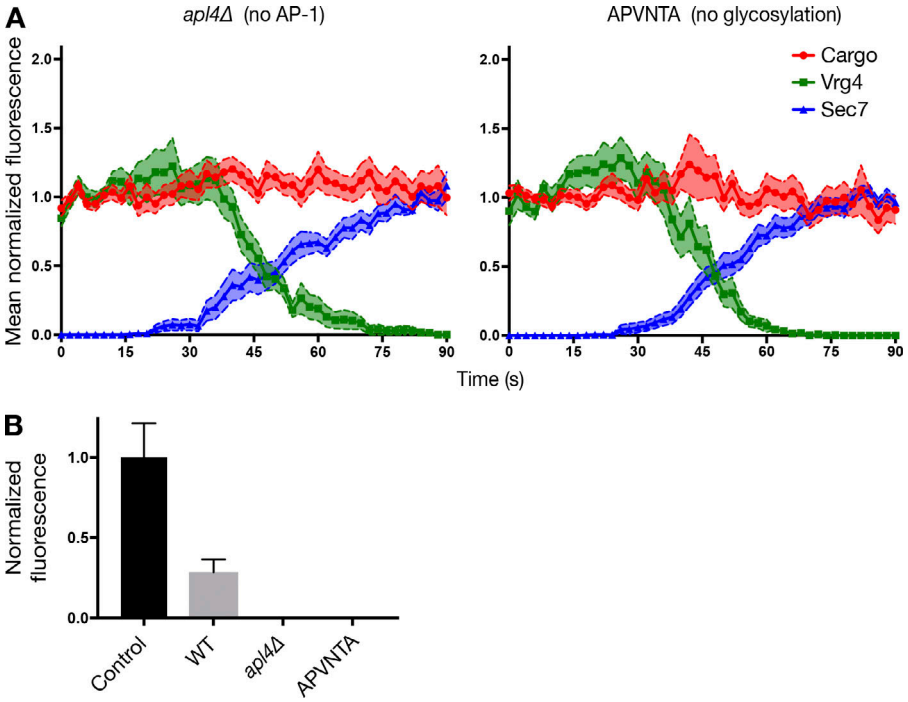

Figure 8. **Suppression of intercisternal transport of the fluorescent secretory cargo. (A)** Fluorescent secretory cargo levels during the early-to-late Golgi transition after eliminating AP-1 or asparagine-linked glycosylation. The analysis was performed as in Fig. 6 C, except that Z-stacks were captured every 2 s. For each yeast strain, 17 early-to-late Golgi transitions visualized in at least nine videos were averaged. Where indicated, the cells lacked AP-1 due to an *apl4Δ* mutation, or the secretory cargo lacked asparagine-linked glycosylation due to the presence of the APVNTA hexapeptide. **(B)** Quantification of the average secretory cargo fluorescence in cisternae of nocodazole-treated daughters at the time of maximal Sec7 signal. The Control measurements were performed using the glycosylated secretory cargo in unbleached cells, and the other three measurements were performed after recovery from bleaching as in Fig. 7. WT, cells with wild-type AP-1 and the glycosylated secretory cargo. The remaining two bars (for which virtually no signals were detected) are from the conditions described in A. Error bars represent SEM for measurements of at least four cisternae for each condition.

This conclusion was somewhat surprising because AP-1 has been implicated in capturing transmembrane cargo proteins by binding their cytosolic tails (Hirst et al., 2012; Myers and Payne, 2013; Whitfield et al., 2016). By contrast, the artificial fluorescent secretory cargo is soluble in the cisternal lumen and is unlikely to contain signals for intra-Golgi recycling. A possible exception is the asparagine-linked oligosaccharide, which is present in four copies in the fluorescent tetramers. Those oligosaccharides could kinetically associate with transmembrane glycosylation enzymes that undergo AP-1–dependent recycling. In support of this possibility, when we tested the nonglycosylated fluorescent secretory cargo containing the APVNTA hexapeptide, there was only a minimal increase in the amount of fluorescent secretory cargo during the early-to-late transition (Fig. 8 A), and no detectable recovery of cargo fluorescence in bleached cisternae (Fig. 8 B). Thus, transport of the fluorescent secretory cargo between cisternae requires both AP-1 and asparagine-linked glycosylation.

Visualizing departure of the secretory cargo from the Golgi

Golgi maturation is believed to terminate with the dissolution of a late Golgi cisterna into transport carriers, including secretory carriers destined for the plasma membrane. We tried to observe this phenomenon by taking rapid 4D confocal videos of the fluorescent secretory cargo in cells that expressed Sec7-HaloTag to mark the late Golgi as well as Apl2-GFP to mark AP-1 (Video 7 and Fig. 9). As we reported previously (Day et al., 2018), AP-1 arrived at late Golgi cisternae later than Sec7 and also departed somewhat later. Fluorescent secretory cargo was often detectable after Sec7 had departed, and disappeared in synchrony with AP-1. However, our microscopy system was unable to track the carriers that transported the fluorescent secretory cargo out of terminally maturing Golgi cisternae. A future challenge is to image the fluorescent secretory cargo as it travels from the late Golgi to the plasma membrane.

Discussion

Although budding yeast is extremely useful for studying membrane traffic, this system has lacked model cargo proteins that could be accumulated in the ER and then tracked by microscopy during their passage through the secretory pathway. For comparison, secretory cargo transport in animal cells has been visualized using model cargo proteins such as procollagen and the thermosensitive tsO45 mutant of vesicular stomatitis virus G protein (Presley et al., 1997; Mironov et al., 2001; Trucco et al., 2004). Those cargo proteins can be accumulated in the ER and then released for exit to the Golgi. A newer method is the retention using selective hooks (RUSH) system, which allows a variety of cargo proteins to be trapped in the ER and then released (Boncompain et al., 2012; Chen et al., 2017). Yet another approach generates reversible aggregates in the ER by fusing four copies of a dimerizing FKBP variant to a GFP-tagged cargo protein (Rivera et al., 2000). Addition of an FKBP ligand dissolves the aggregates and allows the solubilized fluorescent protein to exit the ER. For yeast, we adapted this last strategy with modifications. A dimerizing FKBP variant was fused to the tetrameric fluorescent protein DsRed-Express2 (Strack et al., 2008), and this construct was targeted to the ER lumen with a signal sequence. The result is that the cells accumulate red fluorescent aggregates that can be dissolved to trigger ER exit.

This approach required overcoming a series of technical hurdles to ensure that the fluorescent secretory cargo reaches the ER lumen, that the cargo aggregates dissolve efficiently, and

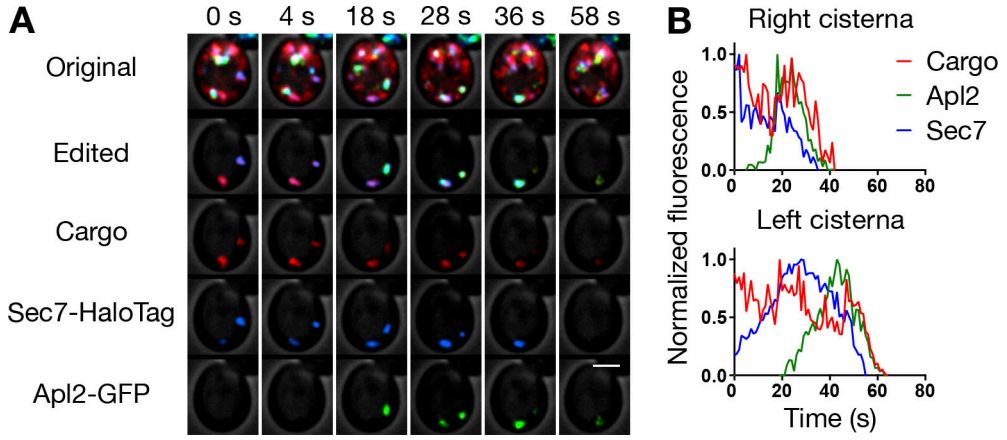

Figure 9. **Departure of the fluorescent secretory cargo from the late Golgi. (A)** Visualizing the cargo in terminally maturing cisternae. Cells expressing the APVNTT-DsRed-Express2-FKBPRD(C22V) cargo together with Sec7-HaloTag and Apl2-GFP were grown to mid-log phase, labeled with JF_{646}, treated with SLF for 5 min, and imaged by 4D confocal microscopy with an interval of 1 s between Z-stacks. Shown are projected Z-stacks from the representative data in Video 7. The top row is the complete projection, the second row is the same projection after editing to highlight the two cisternae that were tracked, and the remaining three rows are the individual channels for the edited projection. Scale bar, 2 µm. **(B)** Quantification of the Golgi markers and the fluorescent secretory cargo for the two cisternae tracked in A. These data are representative of five total videos in which one or more cisternae were analyzed per video.

that the cargo traverses the secretory pathway without being diverted to the vacuole (Casler and Glick, 2018). A key step was to add a tripeptide ER export signal to the cargo (Nam et al., 2014; Yin et al., 2018). As a result, the solubilized cargo exits the ER and passes through the Golgi in a nearly synchronous wave.

The anticipated behavior of this secretory cargo was guided by earlier work with endogenous yeast secretory cargo proteins such as invertase and α-factor (Gaynor and Emr, 1997; Brigance et al., 2000), and with mammalian secretory cargo proteins such as procollagen and vesicular stomatitis virus G protein. We expected that the secretory cargo would appear first in early and then in late Golgi cisternae. As a result of passage through the Golgi, the asparagine-linked oligosaccharide should be modified. Finally, the secretory cargo should be delivered to secretion sites, which for much of the yeast cell cycle are sites of polarized growth (Finger and Novick, 1998). Each of these predictions was confirmed for the fluorescent secretory cargo. The time scale for transit from the ER to the late Golgi is minutes, consistent with the kinetics for transport of α-factor through the yeast secretory pathway (Losev et al., 2006). Thus, by all of the available criteria, our artificial fluorescent fusion protein construct behaves like a bona fide secretory cargo.

Using the fluorescent secretory cargo, we visualized traffic through the yeast secretory pathway, beginning with transfer from the ER to the early Golgi. The prevailing model is that new Golgi cisternae form by the coalescence of COPII vesicles that have encapsulated secretory cargo proteins while budding from ERES. In support of this idea, previous work revealed associations of early Golgi cisternae with ERES in *S. cerevisiae* (Levi et al., 2010; Okamoto et al., 2012; Kurokawa et al., 2014). However, those associations were seen for only a subset of the labeled compartments, and the data were not integrated with studies of maturation kinetics. We now show that early Golgi cisternae form next to the ER, presumably at ERES, and then dissociate from the ER as they mature. Furthermore, within ∼1 min after SLF addition, the fluorescent secretory cargo begins to accumulate in punctate structures that are associated with ERES. Those punctate structures subsequently acquire the early Golgi marker Vrg4. Our interpretation is that the fluorescent secretory cargo exits the ER in COPII vesicles and becomes concentrated in newly forming early Golgi cisternae.

The next step was to track the secretory cargo as a cisterna matured from early to late. This transition can be visualized by using different fluorescent colors to tag the early Golgi marker Vrg4 and the late Golgi marker Sec7 (Losev et al., 2006). To image those two Golgi markers together with the red fluorescent secretory cargo, Vrg4 was tagged with GFP while Sec7 was tagged with HaloTag conjugated to the far-red dye JF_{646} (Grimm et al., 2015). We reproducibly found that a Golgi cisterna labels continuously with the secretory cargo as the cisterna loses Vrg4 and acquires Sec7. This result verifies a core prediction of the cisternal maturation model. Substantially similar results for a yeast membrane protein are reported in the accompanying manuscript in this issue from the Nakano laboratory (Kurokawa et al., 2019).

Continuous labeling of cisternae with a secretory cargo does not necessarily mean that each cargo molecule remains within a particular cisterna. Alternatively, some cargo molecules could exchange between cisternae in vesicles. Possible pathways for intercisternal vesicular traffic of a secretory cargo include COPI-dependent exchange between early Golgi cisternae and clathrin-dependent recycling from late to transitioning cisternae (Orci et al., 2000; Pellett et al., 2013; Papanikou et al., 2015). Initial evidence for intercisternal traffic of our fluorescent secretory cargo came from the finding that around the time of the early-to-late Golgi transition, the amount of secretory cargo within a cisterna typically increases. To test more directly whether the secretory cargo moves between cisternae, we photobleached the cargo molecules in a subset of the early cisternae and then imaged. There was no recovery of fluorescence until the early-to-late transition, at which point there was sudden recovery. The cargo molecules that arrive during the early-to-late transition

likely originate not from the ER but rather from late Golgi cisternae, for the following reasons. First, if the ER were continuing to supply cargo to Golgi cisternae, the fluorescence signal after photobleaching should have recovered gradually throughout maturation instead of recovering suddenly during the early-to-late transition. Second, by the time of the early-to-late transition, a cisterna has dissociated from the ER and is probably no longer competent to receive COPII vesicles. Third, after the increase in cargo signal during the early-to-late transition, the signal often declines during the late stage of maturation, suggesting that late Golgi cisternae are exporting rather than receiving cargo. The combined results fit best with the idea that maturing late Golgi cisternae produce retrograde carriers that recycle certain components, including the fluorescent secretory cargo, to younger cisternae that are undergoing the early-to-late transition (Fig. 10, A and B). A simple computer simulation confirmed that such a recycling pathway could generate a transient increase in the secretory cargo concentration in a maturing cisterna (Fig. 10 C).

What type of carrier recycles the fluorescent secretory cargo? The most likely candidate is vesicles formed with the aid of the AP-1 clathrin adaptor, which functions in an intra-Golgi recycling pathway (Valdivia et al., 2002; Papanikou et al., 2015; Spang, 2015; Day et al., 2018). In support of this hypothesis, disruption of AP-1 abolishes intra-Golgi recycling of the fluorescent secretory cargo even though cisternal maturation is preserved. We were somewhat surprised to see normal Golgi dynamics in the absence of AP-1. A possible explanation is that late Golgi proteins that ordinarily recycle with the aid of AP-1 now reach the plasma membrane and then recycle in endocytic vesicles, which in yeast fuse directly with Golgi cisternae during the early-to-late transition (Day et al., 2018). In any case, the straightforward interpretation of our data are that AP-1 vesicles recycle the fluorescent secretory cargo.

The question then becomes, how is the fluorescent secretory cargo packaged into AP-1 vesicles, which typically incorporate transmembrane cargo proteins that contain cytosolic trafficking signals (Hirst et al., 2012; Myers and Payne, 2013; Whitfield et al., 2016)? One possibility is that the asparagine-linked oligosaccharides on the soluble cargo are kinetically bound to transmembrane glycosylation enzymes, which in turn are packaged into AP-1 vesicles. Indeed, removal of the glycosylation signal from the fluorescent secretory cargo prevents intra-Golgi recycling. This observation leads us to speculate that intra-Golgi recycling of glycosylated secretory cargo proteins is a quality control mechanism to ensure that oligosaccharides are efficiently processed. Further work will be needed to explore the detailed mechanism that drives recycling of the glycosylated fluorescent secretory cargo and to determine whether a similar pathway exists for other secretory cargo proteins.

These findings focus interest on the early-to-late Golgi transition, which is special in that the recycling secretory cargo arrives specifically during this time. We can therefore define a transitional stage of yeast Golgi maturation by the presence of machinery that captures AP-1 vesicles as well as other incoming carriers such as endocytic vesicles (Day et al., 2018). Building on earlier ideas (Day et al., 2013; Papanikou and Glick, 2014;

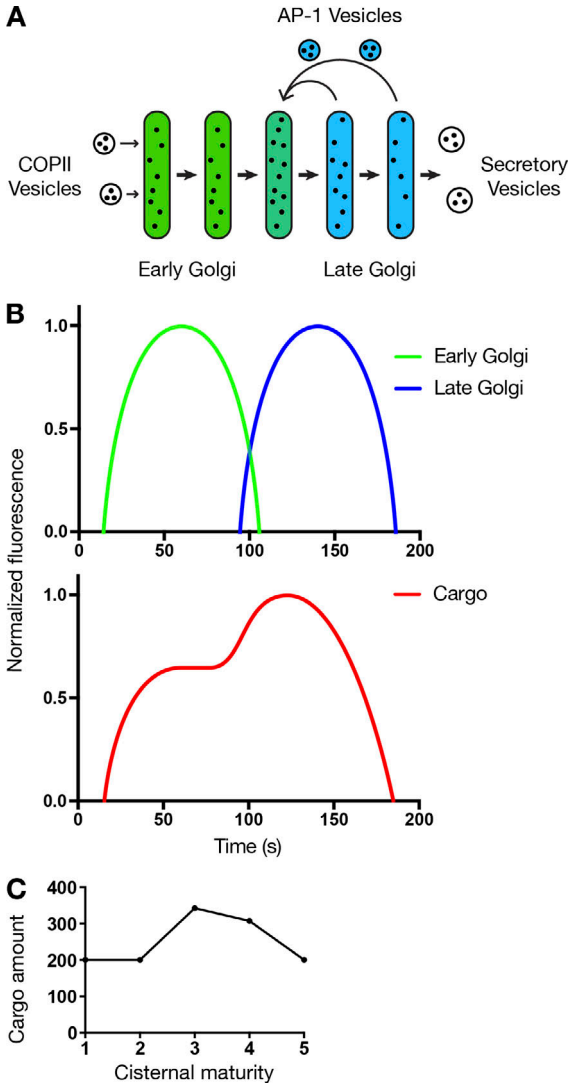

Figure 10. **Secretory cargo traffic during yeast cisternal maturation. (A)** Diagram illustrating the inferred behavior of the fluorescent secretory cargo in maturing yeast cisternae. Green and blue represent early and late resident Golgi proteins, respectively, and black dots represent fluorescent cargo molecules. Progressive maturation is depicted from left to right. The cargo molecules initially travel passively in the maturing cisternae. During the late stage of maturation, a fraction of the cargo molecules recycle in transport vesicles, which are generated with the aid of the AP-1 adaptor, to cisternae that are undergoing the early-to-late transition. **(B)** Qualitative prediction, according to the scheme in A, of the fluorescence signals from resident Golgi proteins and the secretory cargo in a maturing yeast Golgi cisterna. The cargo signal is constant during the early stage of maturation, then rises during the early-to-late transition, then declines during the late stage of maturation. Compare to the simpler scheme in Fig. S1. **(C)** Computer simulation of steady-state cargo levels in maturing Golgi cisternae according to the scheme in A. Details of the simulation procedure are given in Materials and methods. The horizontal axis indicates cisternae of varying maturity, from the newly formed cisterna 1 to the terminally mature cisterna 5. The vertical axis indicates the number of simulated cargo molecules in each cisterna. A cargo molecule in cisterna 4 or 5 could recycle to cisterna 3 with a specified probability. For the simulation shown, the probability of recycling from cisterna 4 was 0.10, and the probability of recycling from cisterna 5 was 0.35, where the increasing probability reflects the late recruitment of AP-1 to the Golgi. Those probability values were chosen for illustrative purposes because they produce a reasonable match to the experimental data, with ~70% more cargo molecules in the transitioning cisterna 3 than in earlier cisternae.

Papanikou et al., 2015; Kim et al., 2016), we envision that Golgi maturation can be divided into early and late stages that produce COPI and clathrin-coated vesicles, respectively, plus an overlapping transitional stage that captures incoming vesicles. This mechanistic view of Golgi organization may be more tractable than the loosely defined concepts of *cis*, medial, *trans*, and *trans*-Golgi network (TGN) compartments.

If intra-Golgi recycling of secretory cargo proteins turns out to be a general phenomenon, it could explain three observations from the literature. First, a study of mammalian cells reported that several secretory cargo proteins exited the Golgi with exponential kinetics rather than with the linear kinetics predicted from a simple maturation scheme (Patterson et al., 2008). The exponential kinetics could be explained by repeated recycling of a fraction of the secretory cargo molecules from late to transitioning cisternae. Second, secretory cargo proteins were found to exchange between Golgi stacks after fusion of mammalian cells (Pellett et al., 2013). That exchange could have been due to intra-Golgi recycling by means of vesicles that traveled long distances in the cytoplasm. Third, an intra-Golgi recycling pathway could explain how certain components accumulate in the TGN even though that compartment turns over rapidly. Accumulation in the TGN can occur when secretory cargo proteins are mutated or incompletely assembled, or when specific components of the trafficking machinery are inactivated (Koval et al., 1997; Gut et al., 1998; von Blume et al., 2012; Guo et al., 2013). Such perturbations may cause the secretory cargo proteins to recycle repeatedly rather than to partition into secretory vesicles. Similarly, when a pulse of a membrane-associated fluorescent dye was internalized to the yeast late Golgi, which is equivalent to the TGN, the dye labeled the late Golgi for much longer than the turnover time of that compartment, implying that membrane was recycling from older to younger cisternae (Day et al., 2018). In yeast, the plasma membrane protein Fus1 can be accumulated in the Golgi by mutations in the exomer complex or in Fus1 itself, and disruption of AP-1 restores transport to the plasma membrane (Barfield et al., 2009), consistent with a role for AP-1 in intra-Golgi recycling of Fus1. A potentially conserved role for mammalian AP-1 in intra-Golgi recycling merits further investigation.

Our results demonstrate the value of using a regulatable fluorescent secretory cargo in a model eukaryote. The same secretory cargo is expected to behave similarly in other cell types, especially because the ER export signal and its cognate receptor are well conserved (Mitrovic et al., 2008; Nam et al., 2014; Saegusa et al., 2018; Yin et al., 2018). For a cell type of interest, if a suitable signal sequence is available to drive cotranslational translocation, and if the SLF ligand can readily penetrate the cells, then it should be possible to achieve aggregation of the fluorescent secretory cargo in the ER followed by rapid transit through the secretory pathway.

Materials and methods

Yeast growth and transformation

The parental haploid *S. cerevisiae* strain was JK9-3da (*leu2-3,112 ura3-52 rme1 trp1 his4*; Heitman et al., 1991). Yeast cells were grown in baffled flasks with shaking at 23°C in non-fluorescent minimal glucose dropout medium (NSD; Bevis et al., 2002) or in rich glucose medium (YPD) supplemented with adenine and uracil. Unless otherwise indicated, cells were grown and imaged in unbuffered NSD. To generate budded cells in which the daughters had yet to inherit nuclei, cells from a logarithmically growing culture were treated for 2 h with 8 µg/ml nocodazole (Thermo Fisher Scientific; AC358240500; stored as a 1,000× stock in DMSO).

The *vps10-104* mutation was generated via pop-in/pop-out mutagenesis as previously described (Fitzgerald and Glick, 2014). Deletion of the *PDR1*, *PDR3*, and *ERV29* genes was accomplished by replacement with a G418, nourseothricin, or hygromycin resistance cassette from pFA6a-kanMX6, pAG25, or pAG32, respectively (Wach et al., 1994; Goldstein and McCusker, 1999). The primers used for amplifying these cassettes were: 5′-CAGCCAAGAATATACAGAAAAGAATCCAAGAAACTGGAAGCGTACGCTGCAGGTCGAC-3′ and 5′-GGAAGTTTTTGAGAACTTTTATCTATACAAACGTATACGTATCGATGAATTCGAGCTCG-3′ for deleting *PDR1*, 5′-ATCAGCAGTTTTATTAATTTTTTCTTATTGCGTGACCGCACGTACGCTGCAGGTCGAC-3′ and 5′-TACTATGGTTATGCTCTGCTTCCCTATTTTCTTTGCGTTTATCGATGAATTCGAGCTCG-3′ for deleting *PDR3*, and 5′-GACTCAAAAAAAGTGAAAACAAAACTGAAAGGATAGATCACGTACGCTGCAGGTCGAC-3′ and 5′-GAGTGAACAGAAGGGACATAAAGAAAAGATTTCCTTTACAATATCGATGAATTCGAGCTCG-3′ for deleting *ERV29*. Yeast cells were transformed with an amplified fragment and selected for resistance to the appropriate antibiotic.

Native yeast proteins were tagged by gene replacement using the pop-in/pop-out method to maintain endogenous expression levels. Secretory cargo proteins were expressed using a *TRP1* integrating vector with the strong constitutive *TPI1* promoter and the *CYC1* terminator (Fitzgerald and Glick, 2014). To ensure similar expression of secretory cargo proteins between strains, single-copy integrants were confirmed by PCR using primers 5′-GTGTACTTTGCAGTTATGACGCCAGATGG-3′ and 5′-AGTCAACCCCCTGCGATGTATATTTTCCTG-3′. All plasmids used in this study are documented in the online supplemental material ZIP file with annotated map/sequence files that can be opened with SnapGene Viewer. Newly generated plasmids have been submitted to Addgene.

Fluorescence microscopy and FRAP experiments

For live-cell fluorescence imaging, yeast strains were grown in NSD (pH ∼4) or in phosphate-buffered NSD at pH 6 and were imaged at room temperature (∼23°C). Where indicated, SLF was diluted from a 100-mM stock in ethanol (Cayman Chemical; 10007974) to a final concentration of 100 µM. For static live-cell imaging, cells were attached to a concanavalin A–coated coverglass-bottom dish containing NSD (Losev et al., 2006) on a Leica SP8 confocal microscope equipped with a 1.4 NA/63× oil objective, using a 60–80-nm pixel size, a 0.25–0.30-µm Z-step interval, and 20–30 optical sections. Z-stacks were captured at intervals of 1–3 s. For 4D live-cell imaging in a flow chamber (Barrero et al., 2016), a 24 × 50-mm coverslip was coated with freshly dissolved 2 mg/ml concanavalin

A (Sigma-Aldrich; C2010) for 10 min, then washed with water and allowed to dry. A 250-µl aliquot of the culture was overlaid on the coverslip, and cells were allowed to adhere for 10 min, followed by several rounds of gentle washing with NSD. The coverslip was placed in the flow chamber and sealed while ensuring that the cells remained immersed in NSD the entire time. NSD was pushed through the flow chamber with a syringe to remove any bubbles, and then the Tygon tubing was clamped. The flow chamber was placed on the stage of an SP8 inverted confocal microscope. One end of the Tygon tubing was connected to a negative pressure pump (Moscovici et al., 2010), while the other end was placed in a culture tube with appropriate medium. To initiate flow of medium, the clamp was removed. Z-stacks were then captured as described above.

For imaging of fixed cells, an aliquot of yeast culture was mixed with an equal volume of 2× ice-cold fixative (100 mM potassium phosphate at pH 6.5, 2 mM $MgCl_2$, 8% formaldehyde, and 0.5% glutaraldehyde) while vortexing. After 1 h on ice, the fixed cells were washed twice with PBS and then resuspended in PBS for viewing.

Static images were converted to 16-bit and average projected (Hammond and Glick, 2000), then range-adjusted to the minimum and maximum pixel values in ImageJ (National Institutes of Health). Movies were deconvolved with Huygens Essential (Scientific Volume Imaging) using the classic maximum likelihood estimation algorithm (Day et al., 2017). Movies were converted to hyperstacks and average projected, then range-adjusted to maximize contrast in ImageJ. Custom ImageJ plugins were used to generate montages of time series, select individual structures and remove background structures, convert edited montages to hyperstacks, and measure fluorescence intensities (Day et al., 2016). Spot tracking was performed using the TrackMate plugin for Fiji.

Perinuclear ER fluorescence was measured as follows (Papanikou et al., 2015). Cells were fixed as described above and then stained with DAPI to mark the nucleus. Cells were compressed under a coverslip, and images of the central regions of the cells, defined along the vertical axis, were collected by wide-field microscopy on a Zeiss Axioplan 2 epifluorescence microscope equipped with a 1.4-NA/100× oil objective and a Hamamatsu digital camera. The DAPI signal was selected using the Magic Wand tool in ImageJ and expanded by 12 pixels to include the nuclear envelope. The cargo signal within this area was then quantified.

FRAP experiments were performed on an SP8 confocal microscope with a 1.4-NA/63× oil objective. Nocodazole-treated cells were adhered to a concanavalin A–coated coverglass-bottom dish and incubated with 100 µM SLF for 3 min before imaging. Daughters (defined by the lack of visible perinuclear ER fluorescence) were selected manually and subjected to photobleaching by 100% intensity laser power at 561 nm. Fluorescence recovery was then monitored by imaging at a standard laser power (5–7%).

HaloTag labeling

To visualize proteins fused to HaloTag, the JF_{646} ligand, kindly provided by Luke Lavis (Janelia Research Campus, Ashburn, VA), was added to 0.5 ml of culture medium to a final concentration of 1 µm from a 1-mM stock in DMSO. The medium was cleared of any precipitate by spinning at 17,000 *g* (13,000 rpm) in a microcentrifuge for 1 min. Then the cleared medium containing the JF_{646} ligand was added to 0.5 ml of yeast culture, and the cells were incubated with shaking at 23°C for 30 min. Excess dye was removed by filtration through and washing on a 0.22-µm syringe filter (Millipore; SLGV004SL). The washed cells were resuspended in NSD and adhered to a concanavalin A–coated coverglass-bottom dish. Videos were captured immediately with an SP8 confocal microscope.

Immunoblotting of yeast cell lysate and secreted protein

A 5- to 25-ml yeast culture was grown in YPD overnight with shaking in a baffled flask to an OD_{600} of 0.7–1.0. The cells were collected by a brief spin in a microcentrifuge, washed twice with fresh YPD, and resuspended in the original volume of fresh YPD. Cultures were treated with 100 µM SLF, and 1.6 ml was removed at each time point. The cells were collected by spinning at 2,500 *g* (5,000 rpm) for 2 min in a microcentrifuge. The culture medium supernatant was transferred to a fresh microcentrifuge tube on ice, and the cells were washed once with deionized water. Then the cells were resuspended in 100 µl PBS. Glass beads (0.5 mm; BioSpec Products) were added to bring the total volume to ∼200 µl, and the sample was vortexed three times for 1 min each separated by 1-min intervals on ice. Finally, 800 µl of PBS was added, the solution was mixed, and 800 µl of the cell lysate was transferred to a fresh microcentrifuge tube.

Protein samples were precipitated using the ND Protein Precipitation Kit (National Diagnostics; EC-888). Briefly, a sample was supplemented with 1/20 volume reagent A followed by 1/10 volume reagent B. Samples were mixed by inversion and incubated at 23°C for 15 min followed by spinning at 17,000 *g* (13,000 rpm) for 10 min in a microcentrifuge. Each pellet was resuspended in 1 ml acetone and spun as before for 15 min, and then the supernatant was removed. The resulting pellet was washed twice with 70% ethanol and resuspended in 50 µl SDS-PAGE sample buffer.

Treatment with endo H was performed as described by the manufacturer (New England Biolabs; P0702S). Briefly, Glycoprotein Denaturing Buffer was added to the protein sample, which was boiled for 5–10 min, followed by addition of GlycoBuffer 3 and endo H. The reaction was performed at 37°C for at least 1 h.

For immunoblotting, 9 µl of each cell lysate and 14 µl of each secreted protein sample were run on a 4–20% Tris-glycine gel (Bio-Rad; 4561094) together with a molecular weight marker (Bio-Rad; Precision Plus Protein Dual Color Standards; 1610374). The separated proteins were transferred to a PVDF membrane (Bio-Rad; 1704156) using the Trans-Blot Turbo system (Bio-Rad). The membrane was blocked with 5% nonfat dry milk in TBST (50 mM Tris-HCl at pH 7.6, 150 mM NaCl, and 0.05% Tween 20) with shaking at room temperature for 1 h, and then incubated with 1:1,000 polyclonal rabbit anti-FKBP12 antibody (Abcam; ab2918, raised against an N-terminal peptide from FKBP) in 5% milk/TBST with shaking overnight at 4°C. After four 5-min washes in TBST, the membrane was incubated with a 1:1,000

dilution of goat anti-rabbit secondary antibody conjugated to Alexa Fluor 647 (Thermo Fisher Scientific; A21245) for 1 h at room temperature. The membrane was then washed twice with TBST and twice with 50 mM Tris-HCl at pH 7.6 and 150 mM NaCl. Analysis was performed with a LI-COR Odyssey CLx imaging system.

Analysis of *HAC1* mRNA splicing

RNA isolation was performed using the Qiagen RNeasy Mini Kit (74104). 1 ml of yeast culture at an OD_{600} of 0.6–0.8 was centrifuged for 1 min at 2,400 *g* (5,000 rpm) in a microcentrifuge. The liquid was removed, and the cell pellet was resuspended in 600 µl of RLT buffer that had been supplemented with 10 µl β-mercaptoethanol per ml of buffer. Cells were lysed by addition of ∼600 µl of glass beads followed by vortexing three times for 1 min each, with intervals of 1 min on ice between rounds of vortexing. After lysis, RNA purification was performed as detailed in the kit handbook.

cDNA synthesis was performed using the ProtoScript II First Strand cDNA Synthesis Kit from New England Biolabs (E6560S). Briefly, 6 µl of the isolated RNA was combined with 10 µl of 2× ProtoScript II Reaction Mix, 2 µl of primer $d(T)_{23}$ VN, and 2 µl of 10× ProtoScript II Enzyme Mix. Samples were incubated at 42°C for 1 h followed by heat inactivation of the enzymes at 80°C for 5 min.

PCR was performed using primers 5′-ACGACGCTTTTGTTG CTTCT-3′ and 5′-TCTTCGGTTGAAGTAGCACAC-3′, which flank the intron of the *HAC1* mRNA. A 10-µl aliquot of each PCR product was subjected to agarose gel electrophoresis.

Computer simulations

A Java program was used to simulate transport of a solubilized cargo through the yeast secretory pathway. Ten thousand simulated cargo molecules were initially located in the ER. During each of step of the simulation, 200 cargo molecules exited the ER. The Golgi was modeled as five cisternae of increasing maturity, where cisternae 1–3 represented the early Golgi, cisternae 3–5 represented the late Golgi, and cisterna 3 represented a transitioning cisterna with properties of both the early and late Golgi. Maturation was modeled as forward movement of the cargo molecules in each cisterna to the next cisterna, or for cisterna 5, as forward movement to a post-Golgi status. To simulate recycling, cargo molecules in cisternae 4 and 5 had specified probabilities of traveling back to cisterna 3 instead of moving forward. After 25 steps of the simulation, half of the cargo molecules had exited the ER, and the system was assumed to be at steady-state. Five thousand simulations of 25 steps each were performed, and the average number of cargo molecules in each location was calculated.

Online supplemental material

Fig. S1 shows our original prediction of how the cargo fluorescence signal would appear in a maturing yeast Golgi cisterna. Fig. S2 shows that the C22V mutation does not affect the ability of reversibly dimerizing FKBP to generate fluorescent aggregates that can be dissolved by SLF, and that the presence of cargo aggregates in the ER does not activate the UPR. Fig. S3 shows evidence that the cargo with the APVNTT export signal experiences a kinetic race between aggregation and ER export, and that increasing the temperature favors ER export over aggregation. Fig. S4 shows that nocodazole has no discernible effect on the operation of the *S. cerevisiae* secretory pathway. Fig. S5 shows that export of the fluorescent cargo from the *S. cerevisiae* ER appears to take place at only a subset of the ERES as marked by COPII. Video 1 shows SLF-induced dissolution of cargo aggregates in the ER lumen. Video 2 shows that cargo secreted in minimal medium is trapped in the periplasm, where the fluorescence can be quenched by lowering the pH of the medium. Video 3 shows an early Golgi cisterna forming near the ER and then dissociating from the ER. Video 4 shows exported secretory cargo concentrating in an early Golgi cisterna that forms in close proximity to an ERES. Video 5 shows that the fluorescent secretory cargo is continuously present in Golgi cisternae as they mature from early to late. Video 6 shows a FRAP experiment documenting that cargo arrives in a cisterna around the time of the early-to-late transition. Video 7 shows fast 4D imaging of terminally maturing cisternae as both the cargo and the late Golgi markers depart. Data S1 ZIP file contains annotated SnapGene files for all of the plasmids used in this study.

Acknowledgments

Thanks for assistance with fluorescence microscopy to Vytas Bindokas and Christine Labno at the Integrated Microscopy Core Facility. Additional thanks to Luke Lavis for providing the JF_{646} dye, and to the Glick laboratory for constructive feedback.

This work was supported by National Institutes of Health (NIH) grant R01 GM104010. J.C. Casler was supported by NIH training grant T32 GM007183. The Integrated Microscopy Core Facility is supported by the NIH-funded Cancer Center Support Grant P30 CA014599.

The authors declare no competing financial interests.

Author contributions: J.C. Casler helped design the experiments, performed all of the experimental analyses, and produced initial drafts of the text and figures. E. Papanikou carried out extensive exploratory studies that laid the foundation for this project. J.J. Barrero refined the tools for generating the regulatable fluorescent secretory cargo. B.S. Glick supervised the project, helped design the experiments, performed the computer simulations, and prepared the final text and figures.

Submitted: 25 July 2018
Revised: 20 December 2018
Accepted: 29 January 2019

References

Appenzeller-Herzog, C., B. Nyfeler, P. Burkhard, I. Santamaria, C. Lopez-Otin, and H.P. Hauri. 2005. Carbohydrate- and conformation-dependent cargo capture for ER-exit. *Mol. Biol. Cell.* 16:1258–1267. https://doi.org/10.1091/mbc.e04-08-0708

Arlt, H., K. Auffarth, R. Kurre, D. Lisse, J. Piehler, and C. Ungermann. 2015. Spatiotemporal dynamics of membrane remodeling and fusion proteins during endocytic transport. *Mol. Biol. Cell.* 26:1357–1370. https://doi.org/10.1091/mbc.E14-08-1318

Barfield, R.M., J.C. Fromme, and R. Schekman. 2009. The exomer coat complex transports Fus1p to the plasma membrane via a novel plasma membrane sorting signal in yeast. *Mol. Biol. Cell.* 20:4985–4996. https://doi.org/10.1091/mbc.e09-04-0324

Barlowe, C., and A. Helenius. 2016. Cargo capture and bulk flow in the early secretory pathway. *Annu. Rev. Cell Dev. Biol.* 32:197–222. https://doi.org/10.1146/annurev-cellbio-111315-125016

Barrero, J.J., E. Papanikou, J.C. Casler, K.J. Day, and B.S. Glick. 2016. An improved reversibly dimerizing mutant of the FK506-binding protein FKBP. *Cell. Logist.* 6:e1204848. https://doi.org/10.1080/21592799.2016.1204848

Barrero, J.J., J.C. Casler, F. Valero, P. Ferrer, and B.S. Glick. 2018. An improved secretion signal enhances the secretion of model proteins from *Pichia pastoris*. *Microb. Cell Fact.* 17:161. https://doi.org/10.1186/s12934-018-1009-5

Bevis, B.J., A.T. Hammond, C.A. Reinke, and B.S. Glick. 2002. *De novo* formation of transitional ER sites and Golgi structures in *Pichia pastoris*. *Nat. Cell Biol.* 4:750–756. https://doi.org/10.1038/ncb852

Beznoussenko, G.V., S. Parashuraman, R. Rizzo, R. Polishchuk, O. Martella, D. Di Giandomenico, A. Fusella, A. Spaar, M. Sallese, M.G. Capestrano, et al. 2014. Transport of soluble proteins through the Golgi occurs by diffusion via continuities across cisternae. *eLife.* 3:e02009. https://doi.org/10.7554/eLife.02009

Beznoussenko, G.V., A. Ragnini-Wilson, C. Wilson, and A.A. Mironov. 2016. Three-dimensional and immune electron microscopic analysis of the secretory pathway in *Saccharomyces cerevisiae*. *Histochem. Cell Biol.* 146:515–527. https://doi.org/10.1007/s00418-016-1483-y

Boncompain, G., S. Divoux, N. Gareil, H. de Forges, A. Lescure, L. Latreche, V. Mercanti, F. Jollivet, G. Raposo, and F. Perez. 2012. Synchronization of secretory protein traffic in populations of cells. *Nat. Methods.* 9:493–498. https://doi.org/10.1038/nmeth.1928

Bonfanti, L., A.A. Mironov Jr., J.A. Martínez-Menárguez, O. Martella, A. Fusella, M. Baldassarre, R. Buccione, H.J. Geuze, A.A. Mironov, and A. Luini. 1998. Procollagen traverses the Golgi stack without leaving the lumen of cisternae: evidence for cisternal maturation. *Cell.* 95:993–1003. https://doi.org/10.1016/S0092-8674(00)81723-7

Brigance, W.T., C. Barlowe, and T.R. Graham. 2000. Organization of the yeast Golgi complex into at least four functionally distinct compartments. *Mol. Biol. Cell.* 11:171–182. https://doi.org/10.1091/mbc.11.1.171

Casler, J.C., and B.S. Glick. 2018. Visualizing secretory cargo transport in budding yeast. *Curr. Protoc. Cell Biol.* https://doi.org/10.1002/cpcb.80

Castillon, G.A., R. Watanabe, M. Taylor, T.M. Schwabe, and H. Riezman. 2009. Concentration of GPI-anchored proteins upon ER exit in yeast. *Traffic.* 10:186–200. https://doi.org/10.1111/j.1600-0854.2008.00857.x

Chen, Y., D.C. Gershlick, S.Y. Park, and J.S. Bonifacino. 2017. Segregation in the Golgi complex precedes export of endolysosomal proteins in distinct transport carriers. *J. Cell Biol.* 216:4141–4151. https://doi.org/10.1083/jcb.201707172

Coorey, N.V.C., J.H. Matthews, D.S. Bellows, and P.H. Atkinson. 2015. Pleiotropic drug-resistance attenuated genomic library improves elucidation of drug mechanisms. *Mol. Biosyst.* 11:3129–3136. https://doi.org/10.1039/C5MB00406C

Cox, J.S., and P. Walter. 1996. A novel mechanism for regulating activity of a transcription factor that controls the unfolded protein response. *Cell.* 87:391–404. https://doi.org/10.1016/S0092-8674(00)81360-4

Daboussi, L., G. Costaguta, and G.S. Payne. 2012. Phosphoinositide-mediated clathrin adaptor progression at the *trans*-Golgi network. *Nat. Cell Biol.* 14:239–248. https://doi.org/10.1038/ncb2427

Dancourt, J., and C. Barlowe. 2010. Protein sorting receptors in the early secretory pathway. *Annu. Rev. Biochem.* 79:777–802. https://doi.org/10.1146/annurev-biochem-061608-091319

Day, K.J., L.A. Staehelin, and B.S. Glick. 2013. A three-stage model of Golgi structure and function. *Histochem. Cell Biol.* 140:239–249. https://doi.org/10.1007/s00418-013-1128-3

Day, K.J., E. Papanikou, and B.S. Glick. 2016. 4D confocal imaging of yeast organelles. *Methods Mol. Biol.* 1496:1–11. https://doi.org/10.1007/978-1-4939-6463-5_1

Day, K.J., P.J. La Rivière, T. Chandler, V.P. Bindokas, N.J. Ferrier, and B.S. Glick. 2017. Improved deconvolution of very weak confocal signals. *F1000 Res.* 6:787. https://doi.org/10.12688/f1000research.11773.1

Day, K.J., J.C. Casler, and B.S. Glick. 2018. Budding yeast has a minimal endomembrane system. *Dev. Cell.* 44:56–72.e4. https://doi.org/10.1016/j.devcel.2017.12.014

De Matteis, M.A., and A. Luini. 2008. Exiting the Golgi complex. *Nat. Rev. Mol. Cell Biol.* 9:273–284. https://doi.org/10.1038/nrm2378

De Nobel, J.G., F.M. Klis, T. Munnik, J. Priem, and H. van den Ende. 1990. An assay of relative cell wall porosity in *Saccharomyces cerevisiae, Kluyveromyces lactis* and *Schizosaccharomyces pombe*. *Yeast.* 6:483–490. https://doi.org/10.1002/yea.320060605

Di Santo, R., S. Aboulhouda, and D.E. Weinberg. 2016. The fail-safe mechanism of post-transcriptional silencing of unspliced *HAC1* mRNA. *eLife.* 5:e20069. https://doi.org/10.7554/eLife.20069

Dunlop, M.H., A.M. Ernst, L.K. Schroeder, D.K. Toomre, G. Lavieu, and J.E. Rothman. 2017. Land-locked mammalian Golgi reveals cargo transport between stable cisternae. *Nat. Commun.* 8:432. https://doi.org/10.1038/s41467-017-00570-z

Dunphy, W.G., and J.E. Rothman. 1985. Compartmental organization of the Golgi stack. *Cell.* 42:13–21. https://doi.org/10.1016/S0092-8674(85)80097-0

Emr, S., B.S. Glick, A.D. Linstedt, J. Lippincott-Schwartz, A. Luini, V. Malhotra, B.J. Marsh, A. Nakano, S.R. Pfeffer, C. Rabouille, et al. 2009. Journeys through the Golgi--taking stock in a new era. *J. Cell Biol.* 187:449–453. https://doi.org/10.1083/jcb.200909011

Field, C., and R. Schekman. 1980. Localized secretion of acid phosphatase reflects the pattern of cell surface growth in *Saccharomyces cerevisiae*. *J. Cell Biol.* 86:123–128. https://doi.org/10.1083/jcb.86.1.123

Finger, F.P., and P. Novick. 1998. Spatial regulation of exocytosis: lessons from yeast. *J. Cell Biol.* 142:609–612. https://doi.org/10.1083/jcb.142.3.609

Fitzgerald, I., and B.S. Glick. 2014. Secretion of a foreign protein from budding yeasts is enhanced by cotranslational translocation and by suppression of vacuolar targeting. *Microb. Cell Fact.* 13:125. https://doi.org/10.1186/s12934-014-0125-0

Galat, A. 2008. Functional drift of sequence attributes in the FK506-binding proteins (FKBPs). *J. Chem. Inf. Model.* 48:1118–1130. https://doi.org/10.1021/ci700429n

Gaynor, E.C., and S.D. Emr. 1997. COPI-independent anterograde transport: cargo-selective ER to Golgi protein transport in yeast COPI mutants. *J. Cell Biol.* 136:789–802. https://doi.org/10.1083/jcb.136.4.789

Glick, B.S., and A. Luini. 2011. Models for Golgi traffic: a critical assessment. *Cold Spring Harb. Perspect. Biol.* 3:a005215. https://doi.org/10.1101/cshperspect.a005215

Glick, B.S., and A. Nakano. 2009. Membrane traffic within the Golgi apparatus. *Annu. Rev. Cell Dev. Biol.* 25:113–132. https://doi.org/10.1146/annurev.cellbio.24.110707.175421

Goldstein, A.L., and J.H. McCusker. 1999. Three new dominant drug resistance cassettes for gene disruption in *Saccharomyces cerevisiae*. *Yeast.* 15:1541–1553. https://doi.org/10.1002/(SICI)1097-0061(199910)15:14<1541::AID-YEA476>3.0.CO;2-K

Grimm, J.B., B.P. English, J. Chen, J.P. Slaughter, Z. Zhang, A. Revyakin, R. Patel, J.J. Macklin, D. Normanno, R.H. Singer, et al. 2015. A general method to improve fluorophores for live-cell and single-molecule microscopy. *Nat. Methods.* 12:244–250. https://doi.org/10.1038/nmeth.3256

Guo, Y., G. Zanetti, and R. Schekman. 2013. A novel GTP-binding protein-adaptor protein complex responsible for export of Vangl2 from the *trans* Golgi network. *eLife.* 2:e00160. https://doi.org/10.7554/eLife.00160

Gut, A., F. Kappeler, N. Hyka, M.S. Balda, H.P. Hauri, and K. Matter. 1998. Carbohydrate-mediated Golgi to cell surface transport and apical targeting of membrane proteins. *EMBO J.* 17:1919–1929. https://doi.org/10.1093/emboj/17.7.1919

Hammond, A.T., and B.S. Glick. 2000. Raising the speed limits for 4D fluorescence microscopy. *Traffic.* 1:935–940.

Heitman, J., N.R. Movva, P.C. Hiestand, and M.N. Hall. 1991. FK 506-binding protein proline rotamase is a target for the immunosuppressive agent FK 506 in *Saccharomyces cerevisiae*. *Proc. Natl. Acad. Sci. USA.* 88:1948–1952. https://doi.org/10.1073/pnas.88.5.1948

Hirst, J., G.H. Borner, R. Antrobus, A.A. Peden, N.A. Hodson, D.A. Sahlender, and M.S. Robinson. 2012. Distinct and overlapping roles for AP-1 and GGAs revealed by the "knocksideways" system. *Curr. Biol.* 22:1711–1716. https://doi.org/10.1016/j.cub.2012.07.012

Holt, D.A., J.I. Luengo, D.S. Yamashita, H.J. Oh, A.L. Konialian, H.K. Yen, L.W. Rozamus, M. Brandt, M.J. Bossard, M.A. Levy, et al. 1993. Design, synthesis, and kinetic evaluation of high-affinity FKBP ligands and the X-ray crystal structures of their complexes with FKBP12. *J. Am. Chem. Soc.* 115:9925–9938. https://doi.org/10.1021/ja00075a008

Ishii, M., Y. Suda, K. Kurokawa, and A. Nakano. 2016. COPI is essential for Golgi cisternal maturation and dynamics. *J. Cell Sci.* 129:3251–3261. https://doi.org/10.1242/jcs.193367

Jacobs, C.W., A.E.M. Adams, P.J. Szaniszlo, and J.R. Pringle. 1988. Functions of microtubules in the *Saccharomyces cerevisiae* cell cycle. *J. Cell Biol.* 107:1409–1426. https://doi.org/10.1083/jcb.107.4.1409

Jørgensen, M.U., S.D. Emr, and J.R. Winther. 1999. Ligand recognition and domain structure of Vps10p, a vacuolar protein sorting receptor in *Saccharomyces cerevisiae*. *Eur. J. Biochem.* 260:461–469. https://doi.org/10.1046/j.1432-1327.1999.00176.x

Kim, J.J., Z. Lipatova, U. Majumdar, and N. Segev. 2016. Regulation of Golgi cisternal progression by Ypt/Rab GTPases. *Dev. Cell.* 36:440–452. https://doi.org/10.1016/j.devcel.2016.01.016

Kornfeld, R., and S. Kornfeld. 1985. Assembly of asparagine-linked oligosaccharides. *Annu. Rev. Biochem.* 54:631–664. https://doi.org/10.1146/annurev.bi.54.070185.003215

Koval, M., J.E. Harley, E. Hick, and T.H. Steinberg. 1997. Connexin46 is retained as monomers in a *trans*-Golgi compartment of osteoblastic cells. *J. Cell Biol.* 137:847–857. https://doi.org/10.1083/jcb.137.4.847

Kurokawa, K., M. Okamoto, and A. Nakano. 2014. Contact of *cis*-Golgi with ER exit sites executes cargo capture and delivery from the ER. *Nat. Commun.* 5:3653. https://doi.org/10.1038/ncomms4653

Kurokawa, K., O. Osakada, T. Kodijani, M. Waga, Y. Suda, H. Asakawa, T. Haraguchi, and A. Nakano. 2019. Visualization of secretory cargo transport within the Golgi apparatus. *J. Cell Biol.* https://doi.org/10.1093/jcb.201807194.

Lavieu, G., H. Zheng, and J.E. Rothman. 2013. Stapled Golgi cisternae remain in place as cargo passes through the stack. *eLife.* 2:e00558. https://doi.org/10.7554/eLife.00558

Levi, S.K., D. Bhattacharyya, R.L. Strack, J.R.I. Austin II, and B.S. Glick. 2010. The yeast GRASP Grh1 colocalizes with COPII and is dispensable for organizing the secretory pathway. *Traffic.* 11:1168–1179. https://doi.org/10.1111/j.1600-0854.2010.01089.x

Lord, C., S. Ferro-Novick, and E.A. Miller. 2013. The highly conserved COPII coat complex sorts cargo from the endoplasmic reticulum and targets it to the Golgi. *Cold Spring Harb. Perspect. Biol.* 5:a013367. https://doi.org/10.1101/cshperspect.a013367

Losev, E., C.A. Reinke, J. Jellen, D.E. Strongin, B.J. Bevis, and B.S. Glick. 2006. Golgi maturation visualized in living yeast. *Nature.* 441:1002–1006. https://doi.org/10.1038/nature04717

Makarow, M. 1988. Secretion of invertase in mitotic yeast cells. *EMBO J.* 7:1475–1482. https://doi.org/10.1002/j.1460-2075.1988.tb02965.x

Maley, F., R.B. Trimble, A.L. Tarentino, and T.H. Plummer Jr. 1989. Characterization of glycoproteins and their associated oligosaccharides through the use of endoglycosidases. *Anal. Biochem.* 180:195–204. https://doi.org/10.1016/0003-2697(89)90115-2

Matsuura-Tokita, K., M. Takeuchi, A. Ichihara, K. Mikuriya, and A. Nakano. 2006. Live imaging of yeast Golgi cisternal maturation. *Nature.* 441:1007–1010. https://doi.org/10.1038/nature04737

Mironov, A.A., G.V. Beznoussenko, P. Nicoziani, O. Martella, A. Trucco, H.S. Kweon, D. Di Giandomenico, R.S. Polishchuk, A. Fusella, P. Lupetti, et al. 2001. Small cargo proteins and large aggregates can traverse the Golgi by a common mechanism without leaving the lumen of cisternae. *J. Cell Biol.* 155:1225–1238. https://doi.org/10.1083/jcb.200108073

Mitrovic, S., H. Ben-Tekaya, E. Koegler, J. Gruenberg, and H.P. Hauri. 2008. The cargo receptors Surf4, endoplasmic reticulum-Golgi intermediate compartment (ERGIC)-53, and p25 are required to maintain the architecture of ERGIC and Golgi. *Mol. Biol. Cell.* 19:1976–1990. https://doi.org/10.1091/mbc.e07-10-0989

Moscovici, M., W.Y. Chien, M. Abdelgawad, and Y. Sun. 2010. Electrical power free, low dead volume, pressure-driven pumping for microfluidic applications. *Biomicrofluidics.* 4:46501. https://doi.org/10.1063/1.3499939

Myers, M.D., and G.S. Payne. 2013. Clathrin, adaptors and disease: insights from the yeast *Saccharomyces cerevisiae*. *Front. Biosci.* 18:862–891. https://doi.org/10.2741/4149

Nam, A.S., Y. Yin, Z. von Marschall, and L.W. Fisher. 2014. Efficient trafficking of acidic proteins out of the endoplasmic reticulum involves a conserved amino terminal IleProVal (IPV)-like tripeptide motif. *Connect. Tissue Res.* 55(Suppl 1):138–141. https://doi.org/10.3109/03008207.2014.923852

Ng, D.T., J.D. Brown, and P. Walter. 1996. Signal sequences specify the targeting route to the endoplasmic reticulum membrane. *J. Cell Biol.* 134:269–278. https://doi.org/10.1083/jcb.134.2.269

Okamoto, M., K. Kurokawa, K. Matsuura-Tokita, C. Saito, R. Hirata, and A. Nakano. 2012. High-curvature domains of the ER are important for the organization of ER exit sites in *Saccharomyces cerevisiae*. *J. Cell Sci.* 125:3412–3420. https://doi.org/10.1242/jcs.100065

Orci, L., M. Ravazzola, A. Volchuk, T. Engel, M. Gmachl, M. Amherdt, A. Perrelet, T.H. Söllner, and J.E. Rothman. 2000. Anterograde flow of cargo across the Golgi stack potentially mediated via bidirectional "percolating" COPI vesicles. *Proc. Natl. Acad. Sci. USA.* 97:10400–10405. https://doi.org/10.1073/pnas.190292497

Otte, S., and C. Barlowe. 2004. Sorting signals can direct receptor-mediated export of soluble proteins into COPII vesicles. *Nat. Cell Biol.* 6:1189–1194. https://doi.org/10.1038/ncb1195

Paetzel, M., A. Karla, N.C. Strynadka, and R.E. Dalbey. 2002. Signal peptidases. *Chem. Rev.* 102:4549–4580. https://doi.org/10.1021/cr010166y

Papanikou, E., and B.S. Glick. 2014. Golgi compartmentation and identity. *Curr. Opin. Cell Biol.* 29:74–81. https://doi.org/10.1016/j.ceb.2014.04.010

Papanikou, E., K.J. Day, J. Austin II, and B.S. Glick. 2015. COPI selectively drives maturation of the early Golgi. *eLife.* 4:e13232. https://doi.org/10.7554/eLife.13232

Patterson, G.H., K. Hirschberg, R.S. Polishchuk, D. Gerlich, R.D. Phair, and J. Lippincott-Schwartz. 2008. Transport through the Golgi apparatus by rapid partitioning within a two-phase membrane system. *Cell.* 133:1055–1067. https://doi.org/10.1016/j.cell.2008.04.044

Pellett, P.A., F. Dietrich, J. Bewersdorf, J.E. Rothman, and G. Lavieu. 2013. Inter-Golgi transport mediated by COPI-containing vesicles carrying small cargoes. *eLife.* 2:e01296. https://doi.org/10.7554/eLife.01296

Pfeffer, S.R. 2010. How the Golgi works: a cisternal progenitor model. *Proc. Natl. Acad. Sci. USA.* 107:19614–19618. https://doi.org/10.1073/pnas.1011016107

Presley, J.F., N.B. Cole, T.A. Schroer, K. Hirschberg, K.J.M. Zaal, and J. Lippincott-Schwartz. 1997. ER-to-Golgi transport visualized in living cells. *Nature.* 389:81–85. https://doi.org/10.1038/38001

Preuss, D., J. Mulholland, A. Franzusoff, N. Segev, and D. Botstein. 1992. Characterization of the *Saccharomyces* Golgi complex through the cell cycle by immunoelectron microscopy. *Mol. Biol. Cell.* 3:789–803. https://doi.org/10.1091/mbc.3.7.789

Rivera, V.M., X. Wang, S. Wardwell, N.L. Courage, A. Volchuk, T. Keenan, D.A. Holt, M. Gilman, L. Orci, F. Cerasoli Jr., et al. 2000. Regulation of protein secretion through controlled aggregation in the endoplasmic reticulum. *Science.* 287:826–830. https://doi.org/10.1126/science.287.5454.826

Rivera-Molina, F.E., and P.J. Novick. 2009. A Rab GAP cascade defines the boundary between two Rab GTPases on the secretory pathway. *Proc. Natl. Acad. Sci. USA.* 106:14408–14413. https://doi.org/10.1073/pnas.0906536106

Rockwell, N.C., D.J. Krysan, T. Komiyama, and R.S. Fuller. 2002. Precursor processing by Kex2/furin proteases. *Chem. Rev.* 102:4525–4548. https://doi.org/10.1021/cr010168i

Rogers, B., A. Decottignies, M. Kolaczkowski, E. Carvajal, E. Balzi, and A. Goffeau. 2001. The pleitropic drug ABC transporters from *Saccharomyces cerevisiae*. *J. Mol. Microbiol. Biotechnol.* 3:207–214.

Rollins, C.T., V.M. Rivera, D.N. Woolfson, T. Keenan, M. Hatada, S.E. Adams, L.J. Andrade, D. Yaeger, M.R. van Schravendijk, D.A. Holt, et al. 2000. A ligand-reversible dimerization system for controlling protein-protein interactions. *Proc. Natl. Acad. Sci. USA.* 97:7096–7101. https://doi.org/10.1073/pnas.100101997

Rossanese, O.W., J. Soderholm, B.J. Bevis, I.B. Sears, J. O'Connor, E.K. Williamson, and B.S. Glick. 1999. Golgi structure correlates with transitional endoplasmic reticulum organization in *Pichia pastoris* and *Saccharomyces cerevisiae*. *J. Cell Biol.* 145:69–81. https://doi.org/10.1083/jcb.145.1.69

Saegusa, K., M. Sato, N. Morooka, T. Hara, and K. Sato. 2018. SFT-4/Surf4 control ER export of soluble cargo proteins and participate in ER exit site organization. *J. Cell Biol.* 217:2073–2085. https://doi.org/10.1083/jcb.201708115

Sato, K., and A. Nakano. 2002. Emp47p and its close homolog Emp46p have a tyrosine-containing endoplasmic reticulum exit signal and function in glycoprotein secretion in *Saccharomyces cerevisiae*. *Mol. Biol. Cell.* 13:2518–2532. https://doi.org/10.1091/mbc.e02-01-0027

Schüller, C., Y.M. Mamnun, H. Wolfger, N. Rockwell, J. Thorner, and K. Kuchler. 2007. Membrane-active compounds activate the transcription factors Pdr1 and Pdr3 connecting pleiotropic drug resistance and membrane lipid homeostasis in *Saccharomyces cerevisiae*. *Mol. Biol. Cell.* 18:4932–4944. https://doi.org/10.1091/mbc.e07-06-0610

Shakoury-Elizeh, M., O. Protchenko, A. Berger, J. Cox, K. Gable, T.M. Dunn, W.A. Prinz, M. Bard, and C.C. Philpott. 2010. Metabolic response to iron deficiency in *Saccharomyces cerevisiae*. *J. Biol. Chem.* 285:14823–14833. https://doi.org/10.1074/jbc.M109.091710

Spang, A. 2015. The road not taken: less traveled roads from the TGN to the plasma membrane. *Membranes (Basel).* 5:84–98. https://doi.org/10.3390/membranes5010084

Strack, R.L., D.E. Strongin, D. Bhattacharyya, W. Tao, A. Berman, H.E. Broxmeyer, R.J. Keenan, and B.S. Glick. 2008. A noncytotoxic DsRed

variant for whole-cell labeling. *Nat. Methods.* 5:955–957. https://doi.org/10.1038/nmeth.1264

Strack, R.L., D. Bhattacharyya, B.S. Glick, and R.J. Keenan. 2009a. Noncytotoxic orange and red/green derivatives of DsRed-Express2 for whole-cell labeling. *BMC Biotechnol.* 9:32. https://doi.org/10.1186/1472-6750-9-32

Strack, R.L., B. Hein, D. Bhattacharyya, S.W. Hell, R.J. Keenan, and B.S. Glick. 2009b. A rapidly maturing far-red derivative of DsRed-Express2 for whole-cell labeling. *Biochemistry.* 48:8279–8281. https://doi.org/10.1021/bi900870u

Tie, H.C., D. Mahajan, B. Chen, L. Cheng, A.M. VanDongen, and L. Lu. 2016. A novel imaging method for quantitative Golgi localization reveals differential intra-Golgi trafficking of secretory cargoes. *Mol. Biol. Cell.* 27:848–861. https://doi.org/10.1091/mbc.E15-09-0664

Toshima, J.Y., S. Nishinoaki, Y. Sato, W. Yamamoto, D. Furukawa, D.E. Siekhaus, A. Sawaguchi, and J. Toshima. 2014. Bifurcation of the endocytic pathway into Rab5-dependent and -independent transport to the vacuole. *Nat. Commun.* 5:3498. https://doi.org/10.1038/ncomms4498

Trimble, R.B., F. Maley, and F.K. Chu. 1983. Glycoprotein biosynthesis in yeast. protein conformation affects processing of high mannose oligosaccharides on carboxypeptidase Y and invertase. *J. Biol. Chem.* 258:2562–2567.

Trucco, A., R.S. Polishchuk, O. Martella, A. Di Pentima, A. Fusella, D. Di Giandomenico, E. San Pietro, G.V. Beznoussenko, E.V. Polishchuk, M. Baldassarre, et al. 2004. Secretory traffic triggers the formation of tubular continuities across Golgi sub-compartments. *Nat. Cell Biol.* 6:1071–1081. https://doi.org/10.1038/ncb1180

Valdivia, R.H., D. Baggott, J.S. Chuang, and R.W. Schekman. 2002. The yeast clathrin adaptor protein complex 1 is required for the efficient retention of a subset of late Golgi membrane proteins. *Dev. Cell.* 2:283–294. https://doi.org/10.1016/S1534-5807(02)00127-2

Vater, C.A., C.K. Raymond, K. Ekena, I. Howald-Stevenson, and T.H. Stevens. 1992. The *VPS1* protein, a homolog of dynamin required for vacuolar protein sorting in *Saccharomyces cerevisiae*, is a GTPase with two functionally separable domains. *J. Cell Biol.* 119:773–786. https://doi.org/10.1083/jcb.119.4.773

von Blume, J., A.M. Alleaume, C. Kienzle, A. Carreras-Sureda, M. Valverde, and V. Malhotra. 2012. Cab45 is required for Ca^{2+}-dependent secretory cargo sorting at the trans-Golgi network. *J. Cell Biol.* 199:1057–1066. https://doi.org/10.1083/jcb.201207180

Wach, A., A. Brachat, R. Pöhlmann, and P. Philippsen. 1994. New heterologous modules for classical or PCR-based gene disruptions in *Saccharomyces cerevisiae*. *Yeast.* 10:1793–1808. https://doi.org/10.1002/yea.320101310

Whitfield, S.T., H.E. Burston, B.D. Bean, N. Raghuram, L. Maldonado-Báez, M. Davey, B. Wendland, and E. Conibear. 2016. The alternate AP-1 adaptor subunit Apm2 interacts with the Mil1 regulatory protein and confers differential cargo sorting. *Mol. Biol. Cell.* 27:588–598. https://doi.org/10.1091/mbc.e15-09-0621

Willer, M., G.M. Forte, and C.J. Stirling. 2008. Sec61p is required for ERAD-L: genetic dissection of the translocation and ERAD-L functions of Sec61P using novel derivatives of CPY. *J. Biol. Chem.* 283:33883–33888. https://doi.org/10.1074/jbc.M803054200

Wooding, S., and H.R.B. Pelham. 1998. The dynamics of Golgi protein traffic visualized in living yeast cells. *Mol. Biol. Cell.* 9:2667–2680. https://doi.org/10.1091/mbc.9.9.2667

Wu, H., B.S. Ng, and G. Thibault. 2014. Endoplasmic reticulum stress response in yeast and humans. *Biosci. Rep.* 34:e00118. https://doi.org/10.1042/BSR20140058

Yin, Y., M.R. Garcia, A.J. Novak, A.M. Saunders, R.S. Ank, A.S. Nam, and L.W. Fisher. 2018. Surf4 (Erv29p) binds amino-terminal tripeptide motifs of soluble cargo proteins with different affinities, enabling prioritization of their exit from the endoplasmic reticulum. *PLoS Biol.* 16:e2005140. https://doi.org/10.1371/journal.pbio.2005140